A well connected, locally-oriented and efficient multi-scale topology optimization (EMTO) strategy

Edouard Duriez, Joseph Morlier, Miguel Charlotte, Catherine Azzaro-Pantel

A well connected, locally-oriented and efficient multi-scale topology optimization (EMTO) strategy

Edouard Duriez[1] · **Joseph Morlier**[1] · **Miguel Charlotte**[1] · **Catherine Azzaro-Pantel**[2]

Abstract
Multi-scale topology optimization (*a.k.a.* micro-structural topology optimization, MTO) consists in optimizing macro-scale and micro-scale topology simultaneously. MTO could improve structural performance of products significantly. However, a few issues related to connectivity between micro-structures and high computational cost have to be addressed, without resulting in loss of performance. In this paper, a new *efficient multi-scale topology optimization* (EMTO) framework has been developed for this purpose. Connectivity is addressed through adaptive transmission zones which limit loss of performance. A pre-computed database of micro-structures is used to speed up the computing. Design variables have also been chosen carefully and include the orientation of the micro-structures to enhance performance. EMTO has been successfully tested on two-dimensional compliance optimization problems. The results show significant improvements compared to mono-scale methods (compliance value lower by up to 20% on a simplistic case or 4% on a more realistic case), and also demonstrate the versatility of EMTO.

Keywords Multi-scale topology optimization · Micro-structure connectivity · Metamodel · Material orientation · Structural database

1 Introduction

1.1 Multi-scale topology optimization

Topology optimization consists in optimizing a structure performance by distributing material within a design space without topological constraints (Bendsoe and Sigmund 2004). This research field now comprises a vast variety of methods: homogenization (Bendse and Kikuchi 1988), Solid Isotropic Material with Penalization (SIMP) (Bendse 1989), evolutionary methods (Xie and Steven 1993), level set methods (Wang et al. 2003), moving morphable components (MMC) (Guo et al. 2014), generalized geometry projection (GGP) (Coniglio et al. 2019), among others. Those methods are described in more detail in Xia et al. (2018) and Norato (2018).

Another approach named *micro-structural design* or *architectured materials design* is based on the same idea but at a micro-scale, leading to macro-scale materials with new apparent and effective properties. The properties are obtained generally by homogenization and can also be optimized. These optimized properties are of many kinds and include for instance terms of the thermo-elasticity tensors (Sigmund 1994) like bulk or shear modulus (Huang et al. 2011), Poisson's ratio (Xie et al. 2014), or thermal expansion (Sigmund and Torquato 1997). This is usually done using periodic boundary conditions (Xia and Breitkopf 2015a).

MTO consists in keeping the best of both micro-scale and macro-scale worlds. The micro-structure of cells is optimized by micro-structural design and those cells are in turn used as macro-elements for a macro-scale topology optimization. A simple way to achieve this is to consider a unique micro-scale topology (Liu et al. 2008; Deng et al. 2013; Yan et al. 2014). However, these approaches do not give results as competitive as with a simple mono-scale topology optimization (Li et al. 2017; Sivapuram et al. 2016). A further step

Responsible Editor: Ole Sigmund

✉ Edouard Duriez
edouard.duriez@isae-supaero.fr

[1] ICA, Université de Toulouse, ISAE-SUPAERO, MINES ALBI, UPS, INSA, CNRS, 3 Rue Caroline Aigle, 31400 Toulouse, France

[2] Laboratoire de Génie Chimique, Université Toulouse, CNRS, INPT, UPS, Toulouse, France

is to consider a small number of micro-scale topologies, for example, one optimized for tension/compression and another one optimized for shearing (Liu et al. 2020b). Although this gives better results, it is still far from being optimal, as the material has to take into account the principal stress orientation for its layout to be optimal (Bendsoe et al. 1994). Having a different micro-structure for each cell enables to follow the orientation of local stress. However, this leads to other problems, namely micro-structure connectivity and computation time.

1.2 Main challenges in MTO

Today, MTO faces two main challenges: one is connecting neighbouring micro-structures without reducing the design space too much, and the other one is acceptable computation times. The micro-structure connectivity issue arises when homogenization is used abusively. Indeed the cell properties obtained through homogenization are meaningful only if all the neighbouring cells share the same structure or at least have very similar structures. However, when cell micro-structure designs spatially vary rapidly, the properties obtained through homogenization are not representative of how the structure will react because two neighbouring micro-structures can be badly connected or disconnected, as in Fig. 1a. In that case, the load transfer is not efficient from a micro-structure to the other.

When a single micro-scale topology is used, connection between micro-structures is not generally a problem especially if density vary smoothly as in Watts et al. (2019) and Wang et al. (2017a). When a small number of micro-scale topologies is used, the issue can be managed by focussing on compatibility between them, as in Liu et al. (2020b). However, being limited to a small number of micro-structures makes it impossible to follow the orientation of local stress.

Other strategies can be implemented for more general cases. For instance, one possibility is to separate cells into spatial groups, or clusters, of same topology in order to ensure connectivity inside those clusters. In that case, connectivity at the cluster interfaces must be managed precisely (Zhou et al. 2019; Du et al. 2018. Another strategy is to impose a non-design zone on the border of every cell to ensure that they will all be connected as in the Kinematical connective Constraint (KC) method (Zhou and Li 2008; Jia et al. 2020) or Qiu et al. (2020), or going further, these zones can be optimized but uniform throughout the structure. However, these two strategies restrict the design space and lead to non-optimal micro-structures. All the micro-structures can also be made connectable during the optimization by coupling their designs (Liu et al. 2020a), but in that case, the coupling of the cells can lead to huge computational time.

Methods using micro-structures that are well adapted to local stress generally have high computational costs, since each individual micro-structure has to be optimized during the global optimization, and this is even worse if the cells are coupled as explained above.

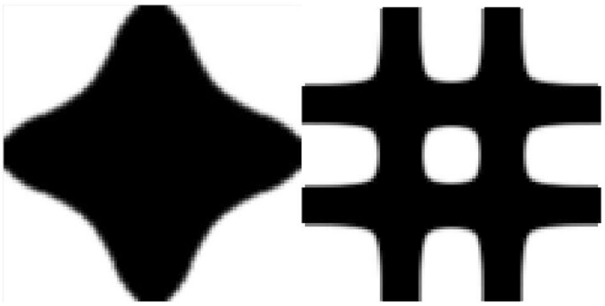

(a) Two badly connected micro-structures : the density is highly discontinuous and the compliance of the assembled micro-structures will therefore be very high

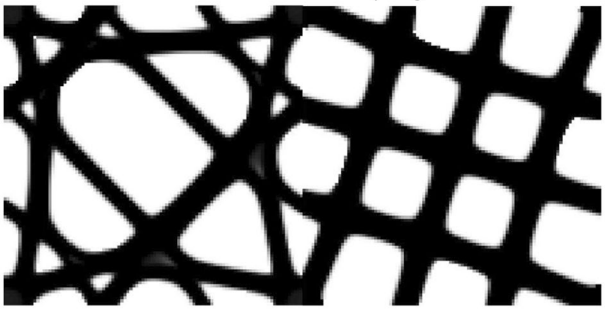

(b) Two well connected micro-structures : the density is sufficiently continuous and only a slight increase in compliance will result from the change of cell structure

Fig. 1 Different qualities of micro-structure connection

These high computational costs can be managed through parallel computing, but the computational costs remain high (Rodrigues et al. 2002; Coelho et al. 2008). Another approach is to approximate the material behaviour using a reduced database model (Xia and Breitkopf 2015b). The micro-structural computations are therefore performed off-line and thus only once. Precomputed databases have also been proposed for parametrized lattice cells. In this case a polynomial model is usually used to access cells in between database points (Wang et al. 2018; Imediegwu et al. 2019; Wang et al. 2020). An alternative is to train a neural network surrogate on the geometrical parameters (White et al. 2019). Using the macro-scale material properties of the micro-structures instead of their geometry as input in the database, enables to vary the topology of the micro-structures (Zhu et al. 2017). A database of pre-computed micro-structures can also be used directly (Ferrer et al. 2018). However, connectivity is not guaranteed in these methods.

The methods mentioned above to ensure connectivity, such as a unique micro-structure design or spatial-clustering, are also a way to lower computational costs but give results that are far from optimal. Other clustering strategies can

lower computational costs such as grouping together cells that have similar densities (Li et al. 2017), similar stress or strain directions (Xu and Cheng 2018), etc. However, the fact that cells are clustered means that their designs cannot be perfectly adapted to the local stress encountered by each cell, and performance is therefore limited. Moreover, clustering that is not based on physical proximity will generally lead back to connectivity issues.

In order to be efficient, a method has therefore to try to address both issues of connectivity and computational cost at the same time while still being adapted to local stress or strain. Rank-two laminates can be used to solve this issue. Those structures have been demonstrated to be optimal for two-dimensional compliance minimization problems (Avellaneda 1987; Allaire et al. 2019). They give therefore excellent results (Jog et al. 1994) but are not easily manufacturable because of the different length scales implied.

An alternative strategy is through variable lattice structures. In that case the topology of the micro-structure will be fixed to a lattice, but the parameters of the lattice are adapted to the local environment (Wang et al. 2017b). For this strategy, the lattice type needs to be chosen carefully. This strategy reduces somewhat the design space but an acceptable performance can be obtained (Wang et al. 2017a). In this last case, a unique micro-structure topology is used but its density as well as the thicknesses of its resulting features vary. In order to have cells that are better adapted to local stresses/strains, and thus to obtain better performances, simple lattices can be oriented with respect to those fields. However, in order to maintain a good connectivity between micro-structures, cosine waves (Groen and Sigmund 2018) and a conformal treatment of orientations are used (Allaire et al. 2019; Li et al. 2020). These methods give generally excellent results. This can be coupled with clustering and generalized to other micro-structures (Kumar and Suresh 2020). In this last case, a non-design region is necessary, leading to sub-optimal designs if one principal stress vanishes. The designs obtained with these methods can then be de-homogenized, meaning that a mechanically well-performing structure is extracted (Stutz et al. 2020).

1.3 MTO formulation

In a two-scale topology optimization formulation, the domain is discretized in n macro-elements, which are themselves discretized in m micro-elements, leading to a total of $m \times n$ micro-elements throughout the domain, as in Fig. 2.

Two types of design variables corresponding to the two scales of optimization are used. The macro-variables correspond to the cell choice: typically, one considers the macro-density x^i_{dens} (with $1 \leq i \leq n$ and $0 < \epsilon \leq x^i_{\text{dens}} \leq 1$) in combination with other macro-variables (x^i_a, x^i_b, …) to

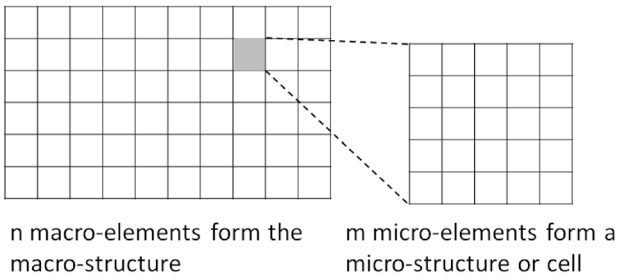

Fig. 2 Illustration of macro-elements and micro-elements in a case where $n = 60$ and $m = 25$ in a rectangular domain

specify hereafter as related to the ith macro-element. Here ϵ has a typical value of 10^{-9}. The considered micro-variable is simply the micro-element density, which is denoted $\rho_{i,j}(x^i_{\text{dens}}, x^i_a, x^i_b, \ldots)$ (with $1 \leq j \leq m$ and $\epsilon < \rho_{i,j} < 1$) for the jth micro-element of the ith macro-element. These micro-densities $\rho_{i,j}$, that are functions of the macro-variables, define the cell structure.

The compliance of the overall structure $c[u] \overset{\text{Def}}{=} u^T K u$ is generally used as objective function, $u(x^i_{\text{dens}}, x^i_a, x^i_b, \ldots)$ being the global displacement vector, and K the global stiffness matrix. Additionally, a global volume fraction constraint is imposed like:

$$\sum_{i=1}^{n} \sum_{j=1}^{m} \rho_{i,j} \leq n \times m \times v_{\text{f}}, \text{ for a given } 0 < v_{\text{f}} < 1$$

In general, the following steps are used to carry out the MTO. In each cell, the current macro-variables are used to access the micro-variable densities $\rho_{i,j}$. The effective micro-element elasticity tensors are derived as $\mathbf{E}_{i,j} = (\rho_{i,j})^p \times \mathbf{E}_0$ from the homogeneous material elasticity tensor $\mathbf{E}_0$ by SIMP interpolation, with a penalization factor of default value $p = 3$. Those tensors are then used to assemble the ith-cell stiffness matrix K_i. The homogenized elasticity tensor of the ith-cell

$$\mathbf{E}^i = \left(E^i_{klpq} \right)_{k,l,p,q \in \{1,2\}} \tag{1}$$

is then derived using the three strain field unit-tests illustrated in Fig. 3. They correspond to two normal strain fields and one shear strain field.

All this process is described in more detail in Xia and Breitkopf (2015a). Those homogenized elasticity tensors are then used at the macro-scale to assemble the global stiffness matrix K of the macro-structure. This matrix is finally inverted to solve the equilibrium problem $u = K^{-1} f$, and compute the global compliance c. The macro-design variables are then updated to start a new iteration.

Equation (2) summarizes the problem being solved.

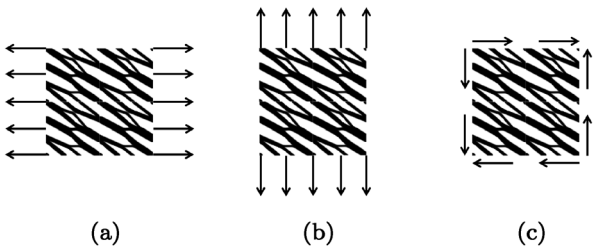

Fig. 3 Unit-test strain fields used for homogenization

$$\underset{x^i_{\text{dens}}, x^i_a, x^i_b, \ldots}{\text{minimize}} \quad u^T K u \tag{2a}$$

$$\text{subject } to \quad Ku = f \tag{2b}$$

$$\sum_{i=1}^{n} \sum_{j=1}^{m} \rho_{i,j} \leq n \times m \times v_{\text{f}} \tag{2c}$$

$$\epsilon < \rho_{i,j} < 1 \tag{2d}$$

This is the problem formulation solved in this paper.

1.4 Main contributions and composition of this paper

In this paper we show that, compared to aforementioned traditional MTO strategies, the use of naturally well connected and oriented micro-structures can significantly improve the structure performance. The main contributions of this paper are:

- Adaptive transition zones resulting in natural connectivity between micro-structures. These transmission zones only slightly reduce the design space compared to unrestricted unit-cell designs (second category in Wu et al. (2021)), thus leading to better performance than micro-structures with a unique topology (Li et al. 2021). They also enable the micro-structures to vary rapidly to adapt to local stress, which is not possible when connectivity is tackled through clustering and interface material (Luo et al. 2021). Unlike other methods in the literature, such as the use of intermediate cells (Hu et al. 2020) or the use of compound cells (Garner et al. 2018), the use of adaptive transmission zones frees us from the need to couple the cells' designs in order for them to be well connected. This in turn enables the cells to be stored in a database.
- A cell database containing not only homogenized properties but also the underlying micro-structures, leading to fast computations. This is made possible by the use of transmission zones.
- Bridging the macro-scale and micro-scale through well chosen variables, including orientation, enabling adaptation of micro-structures to local stresses and a great adaptability to different problem constraints. The use of an orientation variable is different from the de-homogenization approach (Groen and Sigmund 2018; Allaire et al. 2019). Unlike in this approach, the cells aren't rotate to fit in a deformed grid, but rather, the micro-structure is rotated inside the cell. This doesn't lead to lower connectivity, thanks to the use of adaptive transmission zones.

Based on the review by Wu et al. (2021), our approach can be classified as using unrestricted density (category A) but can easily be adapted for a fixed density problem (category C), as is demonstrated in Sect. 4. In terms of restriction on the cell designs, our approach can be classified as using restricted unit-cell designs (category III) because of the adaptive transmission zones. However, because these are not non-design zones, our approach will have a design freedom close to a typical approach using unrestricted unit-cells (category II), as is illustrated in Sect. 2.1. At the same time, we show that three parameters (density, orientation and cubicity) are sufficient to obtain good performance, meaning that we can benefit from the advantages of parameterized unit-cells with multiple parameters (category IV), namely a database of pre-computed cells.

Having already given a description of related works, the rest of this paper is composed as follows.

Section 2 describes how the micro-structures are made to adapt to their environment and connect well with each other. We develop in Sect. 3 our multi-scale strategy. We explain in particular how we use a surrogate cell model based on a database to speed up the optimization, and how we improve performance through post-processing and avoiding local minima. Section 4 provides some comparison to other strategies on classical problems and shows the effectiveness of EMTO. Finally, Sect. 5 concludes the paper by summarizing its main features and suggesting future work. In complement, numerical codes are freely provided as well as companion items for this paper.

2 Connected and adapted micro-structures

2.1 New-adapted variables and objective function

In MTO, the macro-scale and micro-scale topology optimizations are coupled through the macro-scale design variables, which are used as the objective function or the constraints of the micro-scale optimization. For instance, we use the macro-scale density variable (denoted x^i_{dens}) as a constraint on the micro-scale density variables $\rho_{i,j}$ during the micro-scale optimization, as in Eq. (3).

$$\sum_{j=1}^{m} \rho_{i,j} \leq m \times x^i_{\text{dens}} \tag{3}$$

In the simplest forms of MTO, only the density variable is used. However, this leads to generic cells that are not adapted to their environment. Bendsoe et al. (1994) shows that in the case of material and structure simultaneous optimization for minimum compliance, the optimal material is orthotropic with its directions following those of principal strains. Therefore, we choose to add the orientation of the cell as a variable (denoted x^i_{or}). We also add a variable defining the relative importance of the two principal directions. A value of 1 means the two principal directions are equivalent, while a value of 0 means the first principal direction alone is considered. Therefore, we name this variable *cubicity* (denoted x^i_{cub}). Examples of micro-structures obtained for different variable values can be seen in Fig. 4. In this figure, the three variables are successively made to vary, based on an initial cell whose density value is 0.5, orientation angle value is 0, and cubicity value is 0.

In order to obtain these cells, we use the work of Xia and Breitkopf (2015a). In this work, an energy-based homogenization approach is used and the 4D homogenized stiffness tensor $\mathbf{E}^i$ of the ith-macrocell is obtained by Eq. (4)

$$E^i_{klpq} = \frac{1}{m} \sum_{j=1}^{m} (u^{A(kl)}_{ij})^T k_{ij} u^{A(pq)}_{ij} \tag{4}$$

where m is the number of finite elements representing the cell micro-structure, k_{ij} is the stiffness matrix of micro-element j of the ith-macrocell, and $u^{A(pq)}_{ij}$ are the displacement solutions corresponding to the unit-test strain fields in Fig. 3 for micro-element j of the ith-macrocell. In this figure, unit-test strain fields (a), (b) and (c) correspond respectively to (p,q)=(1,1), (2,2) and (1,2). We change the original objective function as follows. First, instead of using directly the 4D homogenized stiffness tensor $\mathbf{E}^i$ of the ith-macrocell, we transform that tensor as in Eq. (5a)

$$\mathbf{E}^{i\alpha} = \mathbf{M}^T_\alpha \times \mathbf{E}^i \times \mathbf{M}_\alpha \equiv (E^{i\alpha}_{klpq})_{k,l,p,q \in \{1,2\}} \tag{5a}$$

$$c_i = E^{i\alpha}_{1111} \times (1 - \frac{x^i_{\text{cub}}}{2}) + E^{i\alpha}_{2222} \times \frac{x^i_{\text{cub}}}{2} \tag{5b}$$

using a rotation tensor $\mathbf{M}_\alpha$. $\mathbf{M}_\alpha$ is defined for a rotation angle $\alpha = x^i_{\text{or}}$ measured with respect to a chosen global basis vector. The ith-macrocell objective function c_i in Eq. (5b) combines then the stiffness component terms for that rotation as well as the ith-macrocell cubicity variable denoted x^i_{cub}. In the codes named *topMulti.m* and *cellOptim.m* (accessible through a link at the end of the paper), the 2D matrix notation of the stiffness tensors ($\mathbf{E}^i$, $\mathbf{E}^{i\alpha}$) is used everywhere, except in the rotation function where the 4D tensor shape is used.

Taking into account the orientation and relative importance of the two principal directions enables intermediate densities to be much less penalized than in the case of a generic cell. This can be seen in Fig. 5, where these oriented cells are compared to a quasi-isotropic cell or to the theoretical Hashin–Shtrikman bound (Hashin and Shtrikman 1962), in terms of $E^{i\alpha}_{1111}$.

Equation (6) summarizes the problem being solved at the micro-scale to obtain the ith ith-macrocell.

$$\underset{\rho_{i,j}}{\text{minimize}} \quad c_i = E^{i\alpha}_{1111} \times (1 - \frac{x^i_{\text{cub}}}{2}) + E^{i\alpha}_{2222} \times \frac{x^i_{\text{cub}}}{2} \tag{6a}$$

$$\text{subject to} \quad K_i u^{A(pq)}_i = f^{(pq)}_i \tag{6b}$$

$$\sum_{j=1}^{m} \rho_{i,j} \leq m \times x^i_{\text{dens}} \tag{6c}$$

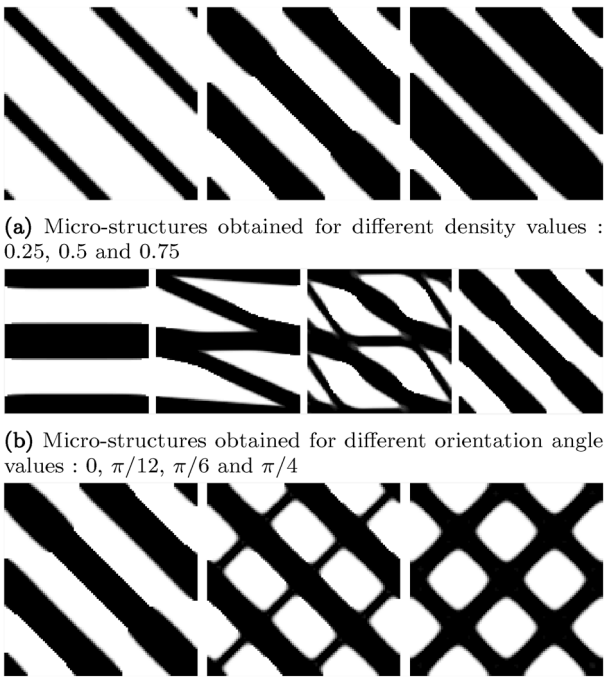

(a) Micro-structures obtained for different density values : 0.25, 0.5 and 0.75

(b) Micro-structures obtained for different orientation angle values : 0, $\pi/12$, $\pi/6$ and $\pi/4$

(c) Micro-structures obtained for different cubicity values : 0, 0.5 and 1

Fig. 4 Influence of the 3 macro-design variables on a micro-structure with an initial density of 0.5, an initial orientation angle of $\pi/4$, and an initial cubicity of 0. In each subfigure, two of these variables are fixed, while the third varies

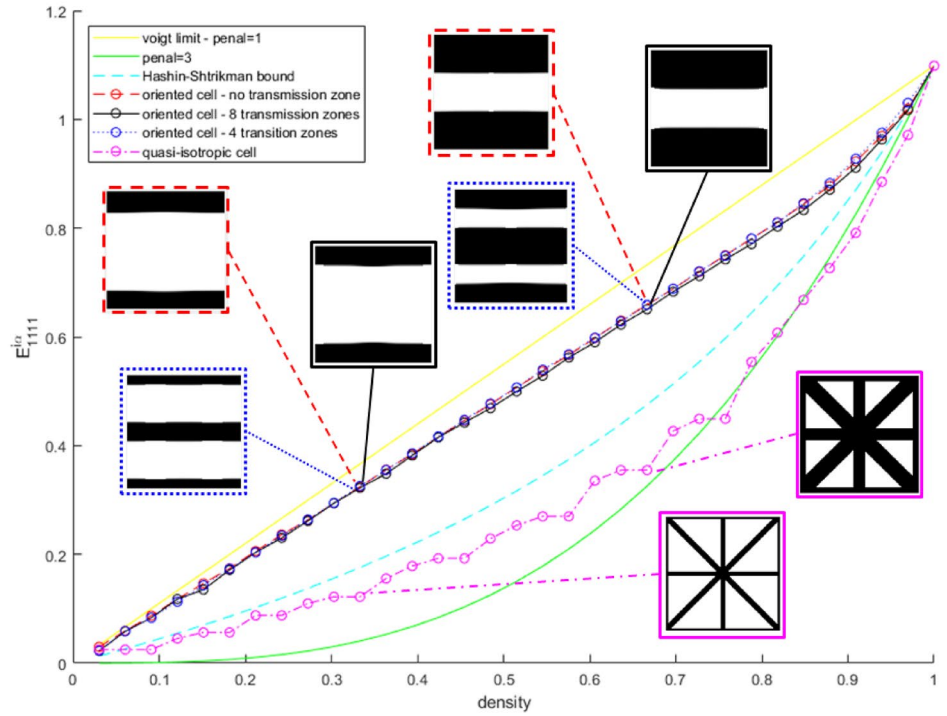

(a) Orientation angle of 0

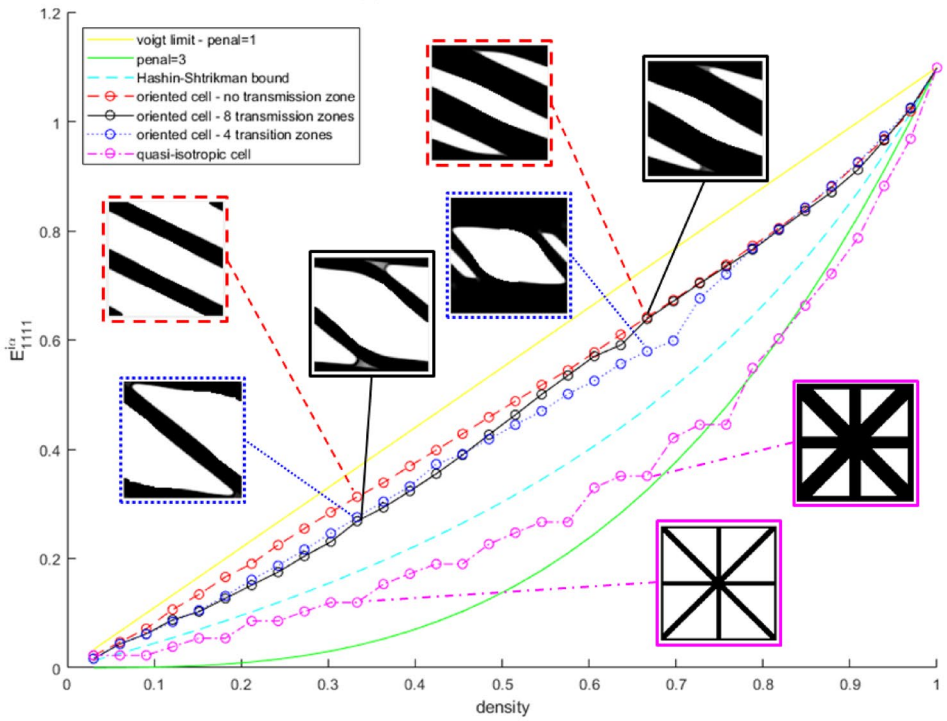

(b) Orientation angle of $\pi/8$

Fig. 5 Comparison of $E^{i\alpha}_{1111}$ (first term of the rotated stiffness tensor) for different cells and at different densities in a uni-directional case. The designs are shown for densities of 1/3 and 2/3. The connectivity constraint lowers very slightly the performance compared to a cell without transmission zones. Far better performances are obtained with oriented cells compared to theoretical isotropic cells (Hashin–Shtrikman bound) or an example of quasi-isotropic cell

$$\epsilon < \rho_{i,j} < 1 \tag{6d}$$

where K_i is the ith-macrocell assembled stiffness matrix, $u_i^{A(pq)}$ and $f_i^{(pq)}$ are the global displacement vector and the external force vector of the ith-macrocell for the case (pq) respectively, $\rho_{i,j}$ is the density of the jth micro-element of the ith-macrocell.

In all the results presented in Sect. 4, micro-structures of size 100×100 are used.

2.2 Micro-structure connection

As seen previously, well-oriented cells are not sufficient to guarantee the good performance of the whole structure. Indeed, homogenization theory can give results far from reality if micro-structures are not well connected. By referring to the definition of connectivity from Wang et al. (2017a), neighbouring micro-structures can be connected without overhanging regions, but there may be some material mismatch. Indeed, as can be seen in Fig. 1a, overhanging regions exhibited by badly connected micro-structures will prevent stresses from being effectively transmitted from one cell to another. As a result, stiffnesses derived from homogenization theory will be overestimated. On the contrary, well connected micro-structures, as in Fig. 1b will pass stresses along effectively.

For this, we choose a number of connection points, pictured in red in Figs. 6. The cell in Fig. 6a has 4 transmission points (2 per edge), whereas the cell in Fig. 6b has 12 transmission points (4 per edge). The stresses will be forced to transit from a micro-structure to its neighbours through these points. In order to enforce that condition, we change the original periodic boundary conditions described in the work of Xia and Breitkopf (2015a). Instead of applying them on all the edge elements of the cell, we only apply them to a specific zone around each transmission points. Those zones are named transmission zones. They are defined as all the edge elements attached to the corresponding transmission point. An edge element is attached to a transmission point if no unused element, lies between them; an unused element being one whose density is below a certain threshold. In the rest of this paper, we use a density threshold of 0.5. For example, in Fig. 6b, there are four transmission zones on the top edge of the cell: the first ranges from the first element (leftmost) to the element labelled 0, the second ranges from the element labelled 1 to the element labelled 2, the third ranges from the element numbered 3 to the one labelled 4, and the last zone ranges from the element numbered 5 to the last element (rightmost).

The number of transmission points has to be chosen before the optimisation process and must be the same for all the cells in the structure, because two cells with a different number of transmission points would be badly connected. A higher number of transmission points will enable micro-structures to be more locally-adapted. Indeed, there will be more possibilities in that case for the micro-structure to connect different transmission points and be aligned with the local principal directions. This leads to better homogenized properties. However, a higher number of transmission points also means that stresses may be transmitted unequally through different transmission points. This means that neighbouring micro-structures will be connected less effectively, leading to lower global performance of the structure. A

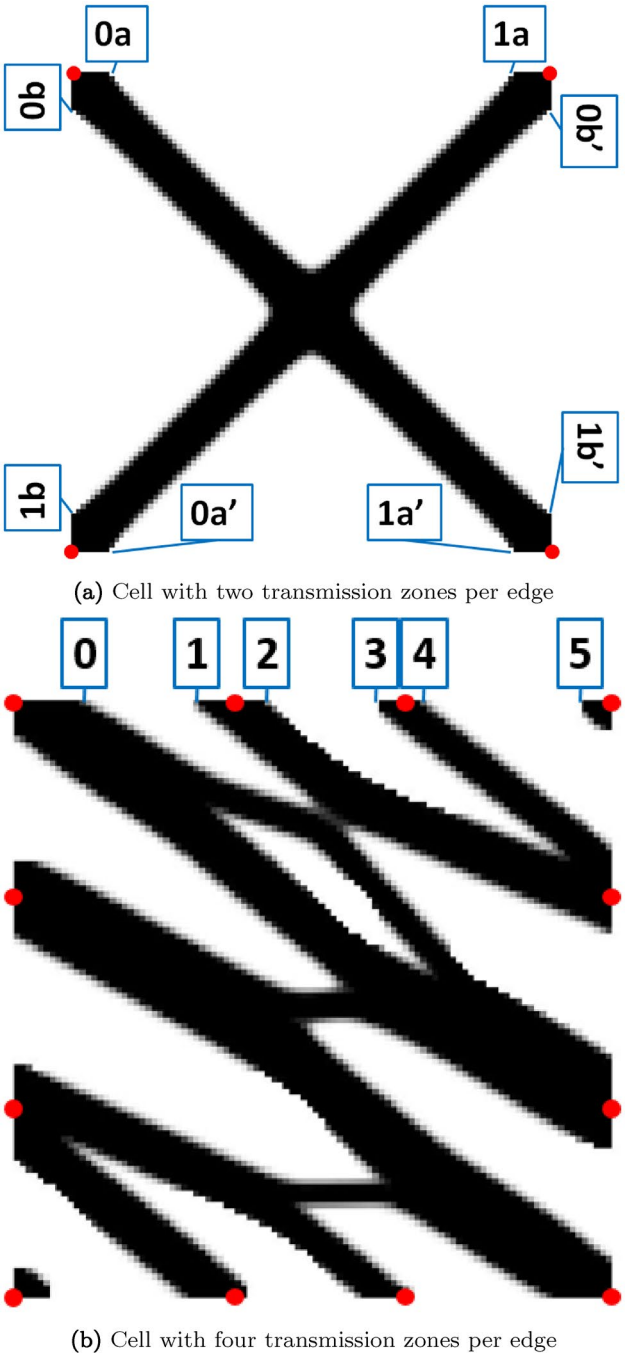

(a) Cell with two transmission zones per edge

(b) Cell with four transmission zones per edge

Fig. 6 Transmission zones of adaptable lengths: all edge micro-elements connected to the transmission points (red) are part of the transmission zones. (Color figure online)

number of two to three transmission points per cell edge seems to give the best overall performance, according to preliminary results.

It is worth noting that, although these transmission zones may seem visually to reduce the design space a lot, they actually only have a very low impact on the cell performance, as can be seen in Fig. 5. This impact on cell

performance is accepted as it increases connectivity dramatically and therefore improves overall performance, as shown in Sect. 4.

Although the lengths of transmission zones vary from a cell to another, their position is the same in every cell. This means that micro-structures are intrinsically connected to each other. As a result the cell designs are uncoupled, meaning that they can be computed in a parallel framework or computed in an off-line approach for creating a database for surrogate modelling (Bouhlel et al. 2019).

Within a cell, some transmission zones could be dominated by others, as in the cells of Fig. 7. From a homogenization point of view, this means that more stress transits through the dominating transmission zones than through the dominated ones. If two cells with similar macro-variables have different dominating transmission zones, they will not be well connected, as in Fig. 7. In order to avoid that issue, it is necessary that no transmission zone be dominant. To ensure this, the micro-structures are first imposed to be symmetric about their central point, which does not impact their performance. The cells are also imposed to use the transmission zones located in the corners of the cells and the other transmission zones equally.

This strategy of transmission zones has similarities with the KC method in Zhou and Li (2008). One of the main differences is that, in our strategy, the transmission zones are not real non-design zones, as their size changes. This means that EMTO can explore more creative designs, as the design space is less reduced.

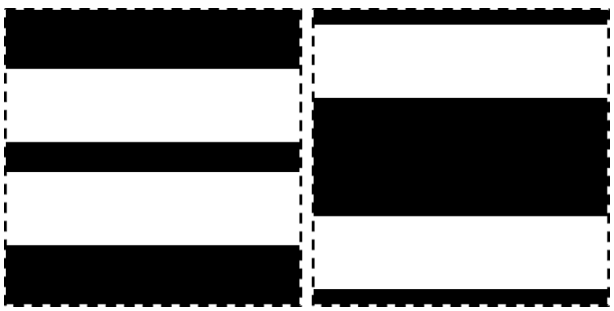

Fig. 7 Illustration of two micro-structures obtained without anti-domination constraints for the same macro-variables : density of 0.5, orientation angle of 0 and cubicity of 0. The transmission zones in the corners of the left cell dominate its other transmission zones, whereas the other transmission zones of the right cell dominate the transmission zones in its corners. Those cells would be badly connected. This illustrates the need for anti-domination constraints

3 Multi-scale strategy

3.1 Micro-structural database construction

In order to take advantage of the properties of the cells described in Sect. 2, a cell database is constructed off-line once and for all with the aim to be then used in every macro-scale optimization. The inputs of this database are the three macro-scale design variables: density, orientation and cubicity. The outputs of this database are the six independent terms of the homogenized stiffness tensor obtained by solving the micro-scale optimization problem presented in Sect. 2.1. The corresponding micro-structures are also stored in a database. This is represented in Fig. 8. Examples of outputs for three random inputs can be found in Appendix 3. This database is built on a regularly-spaced 3-dimensional grid of the three macro-scale design variables in order to have micro-structures close to any point in the design space. Each variable is given 32 values, leading to 32^3 =32,768 different entries, or sets of macro-scale design variables. For each of these entries, the optimum topology is computed following the methodology described in Sect. 2.

However, the micro-structure optimizations are gradient-based, and therefore only find local minima. This leads to high variability in final designs and properties of cells with similar macro-scale variables. These noisy cell properties would be very detrimental to gradient-based macro-scale optimization. To prevent this, a multi-start strategy is used: different initial designs are tested for each set of macro-scale variables (i.e. each cell), and the final micro-structure with the lowest objective function value is kept. Those designs can be seen in Appendix 2 and are created in the Matlab code named *initDes.m* available in the link in Sect. 5.

The orientation variable is given 32 values between 0 and $\pi/4$ rad. The cells corresponding to orientation angles of $\pi/4$ to π are derived by axial symmetry and added to the database. Cells corresponding to a density of 0 and 1 and computed only once and added to the database afterwards.

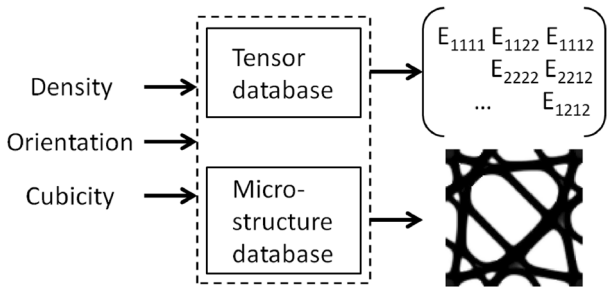

Fig. 8 Scheme of the two databases illustrating the inputs and outputs

This leads to a total of 136000 cells contained in the database.

This database is included in our multi-scale strategy. Our macro-scale topology optimization code is adapted from *top88*, a classical mono-scale topology optimization code (Andreassen et al. 2011). However, instead of density being the only macro-design variable for each macro-element, we add a variable for orientation and cubicity. At each iteration, the stiffness matrix of each macro-element, or cell, is derived from those macro-design variables using the stiffness tensor database. In a MTO process where N_i macro-level iterations are needed and n macro-elements are used, this means that $N_i \times n$ micro-level optimizations would be needed without a database. This number is in the order of tens of thousands in the simple examples shown in Sect. 4. Therefore, a lot of computation time is saved through the use of this database. This results in the micro-optimization and macro-optimization not being concurrent. The workflow is more precisely described in Fig. 9.

3.2 Surrogate prediction

To retrieve a stiffness tensor for a given set of macro-level design variables ($x^i = [x^i_{\text{dens}}, x^i_{\text{or}}, x^i_{\text{cub}}]$), we use the Nadaraya–Watson kernel-weighted average (Nadaraya 1964) with a Gaussian Kernel G, which read as

$$\mathbf{E}_{\text{pred}}(x^i) = \frac{\sum_{l=1}^{k} G(x^i, x_l)\mathbf{E}_{\text{db}}(x_l)}{\sum_{l=1}^{k} G(x^i, x_l)} \tag{7a}$$

$$G(x^i, x_l) = \exp\left(\frac{-d_{\text{eucl}}(x^i, x_l)^2}{2b^2}\right) \tag{7b}$$

In Eq. (7), $\mathbf{E}_{\text{pred}}(x^i)$ is the predicted stiffness tensor of the cell corresponding to x^i; x_l are the points in the database; $\mathbf{E}_{\text{db}}(x_l)$ are the database stiffness tensors of the cells corresponding to those points, and b is the kernel radius;

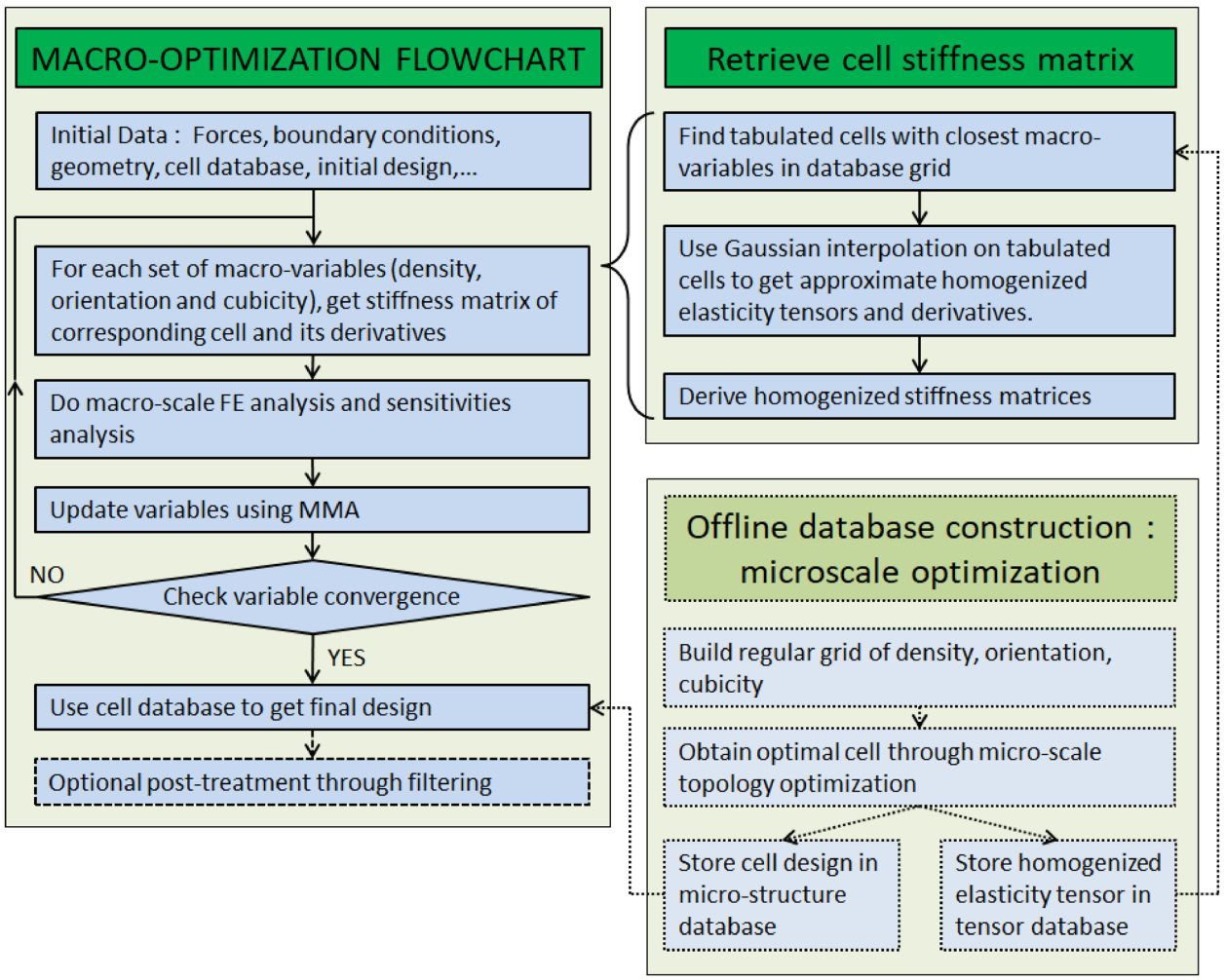

Fig. 9 Macro-optimization workflow

$d_{\text{eucl}}(x^i, x_l)$ measures the Euclidean distance between x^i and x_l.

The foregoing kernel-weighted average provides a regressed stiffness tensor and, for sufficient computational efficiency, is applied on the k cells whose coordinates are within a distance of three kernel radii from the point x^i where a prediction is sought. We set the kernel radius as $b = 0.04$, meaning that around 3000 cells are considered for each regression. This is a compromise between precision and filtering the noise that was not suppressed by the multi-start strategy. The same method is applied to $x^{i\prime} = [x^i_{\text{dens}} + \Delta, x^i_{\text{or}}, x^i_{\text{cub}}]$, $x^{i\prime\prime} = [x^i_{\text{dens}}, x^i_{\text{or}} + \Delta, x^i_{\text{cub}}]$ and $x^{i\prime\prime\prime} = [x^i_{\text{dens}}, x^i_{\text{or}}, x^i_{\text{cub}} + \Delta]$ in order to obtain three other regressed stiffness tensors and be able to derive the partial derivatives through finite differences, as hereafter in Eq. (8), and using $\Delta = 0.01$.

$$\frac{\partial \mathbf{E}_{\text{pred}}}{\partial x_{\text{dens}}}(x^i) \approx \frac{\mathbf{E}_{\text{pred}}(x^{i\prime}) - \mathbf{E}_{\text{pred}}(x^i)}{\Delta} \tag{8a}$$

$$\frac{\partial \mathbf{E}_{\text{pred}}}{\partial x_{\text{or}}}(x^i) \approx \frac{\mathbf{E}_{\text{pred}}(x^{i\prime\prime}) - \mathbf{E}_{\text{pred}}(x^i)}{\Delta} \tag{8b}$$

$$\frac{\partial \mathbf{E}_{\text{pred}}}{\partial x_{\text{cub}}}(x^i) \approx \frac{\mathbf{E}_{\text{pred}}(x^{i\prime\prime\prime}) - \mathbf{E}_{\text{pred}}(x^i)}{\Delta} \tag{8c}$$

The stiffness matrices of the 4-node quadrilateral finite elements representing the cells, and their derivatives, are then derived from the stiffness tensors using four Gauss' points for integration. Those element stiffness matrices are then used to build the global stiffness matrix and follow on with classical mono-scale topology optimization.

Matrices interpolated from a database can loose positive definiteness (Kumar et al. 2021). For every case that is presented in this paper, we checked the positive definiteness of every surrogate elastic tensor throughout the optimization, using Sylvester's criterion. All were positive definite. We think that this is due to our Gaussian kernel surrogate and to the fact that we have a very large database.

3.3 Avoiding local minima

In order to avoid local minima on the border of the design space, a few actions have to be taken to artificially extend the design space. These actions are described hereafter.

The simplest way to manage the variables, is to have the orientation variable range from 0 to π and the cubicity variable range from only one principal direction considered (value of 0) to both principal directions being as important (value of 1). This means that in order to move from a set of variables describing a cell where one of the two principal directions is slightly more important to a set of variable describing a cell where it is the other principal direction that is slightly more important, the orientation variable has to change abruptly by $\pi/2$. For example, the third cell in Fig. 10a has a variable set of [0.5, 0, 0.8], whereas the fifth one has a variable set of [0.5, $\pi/2$, 0.8]. The cell in between could alternatively be described by the sets [0.5, 0, 1] or [0.5, $\pi/2$, 1]. This introduces discontinuities which are detrimental for the gradient-based optimization approach. Indeed, we use the method of moving asymptotes (MMA) to solve the macro-scale topology optimization problem in this work (Svanberg 1987).

In order to correct that discontinuity, the cubicity variable is extended and normalized so that a value of 0 or 1 means that only one or the other principal directions is important, whereas a value of 0.5 means that both principal directions are as important. With this change it is now possible to move from the third cell of Fig. 10a to the fifth one only by a slight change in cubicity. This means that all cells now have two sets of variables pointing to them: $[x_{\text{dens}}, x_{\text{or}}, x_{\text{cub}}]$ and $[x_{\text{dens}}, x_{\text{or}} \pm \pi/2, 1 - x_{\text{cub}}]$. The design space is therefore redundant and has been extended artificially. It also means that there are multiple paths from a cell to another, as can be seen in Fig. 10. This leads to better macro-scale optimizations.

Another local minimum located on the border of the design space is due to the orientation variable. Indeed, if the optimum value of this variable is located on the other side of the range, gradient-based optimization will lead the variable in the wrong direction, as illustrated schematically in Fig. 11a. A first idea to solve this is to extend the design space with redundant values of orientation angles,

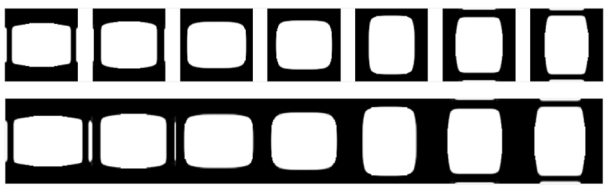

(a) Microstructures obtained for density=0.5, orientation angle=0 and new cubicity values ranging from 0.2 to 0.8

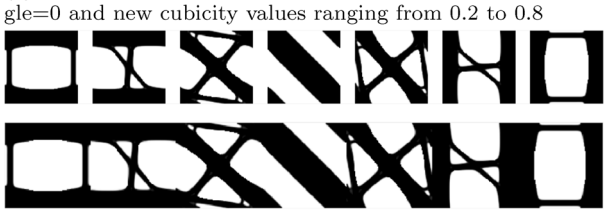

(b) Microstructures obtained for density=0.5, cubicity=0.2 and angle values ranging from 0 to $\pi/2$

Fig. 10 Example showing the redundant design space in order to delete some local minima. There are two paths from the cell on the left (density = 0.5, orientation = 0, cubicity = 0.2) to the cell on the right (density = 0.5, orientation = 0, cubicity = 0.8 or density = 0.5, orientation = $\pi/2$, cubicity = 0.2 depending on the path followed)

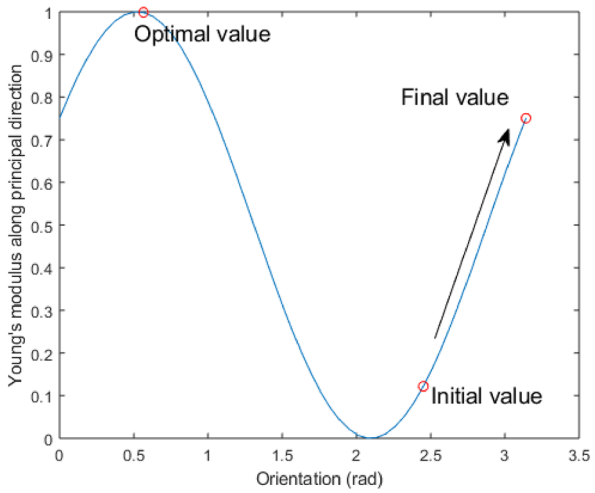

(a) Gradient based optimisation issue : due to the periodic nature of orientation, the optimal value cannot be found with a simple orientation variable.

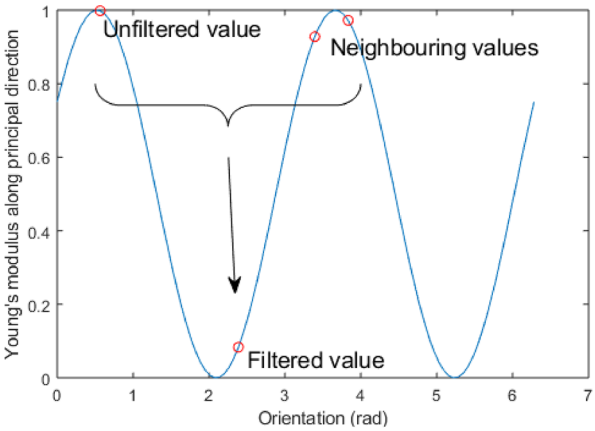

(b) Filtering issue : due again to the periodic nature of orientation a simple filtering method will behave badly

Fig. 11 Issues encountered when dealing with the orientation variable. To solve these issues the orientation macro-variable was replaced with two variables proportional to the orientation cosine and sine

as in Fig. 11b. This way, the optimal orientation value will be reached whatever the initial point in the original design space.

However, there is another issue with the orientation variable due to filtering. Indeed, in our multi-scale framework, all the macro-scale variables are spatially filtered. This can lead to bad values for periodical variables as orientation. More precisely, neighbouring cells can have optimal orientation values that are separated by a period or more, as schematically illustrated in Fig. 11b. In this case the filtered value of this variable will be in between two optimal values, and display very bad properties. For this reason, extending the range of the orientation variable cannot be a good practical solution.

A better way to deal with this problem is to replace the orientation variable x_{or} by two variables $x_{\cos}$ and $x_{\sin}$, from which the orientation is derived as in Eq. (9).

$$x_{\text{or}} = \arctan\left(\frac{x_{\sin}}{x_{\cos}}\right) \tag{9}$$

In this case, the orientation is no more stuck in a local minimum on the border of the design space. In order not to add an additional constraint on these variables, they are not made to respect $x_{\cos}^2 + x_{\sin}^2 = 1$. As a result, these variables are not the real cosine and sine of the orientation angle, but their ratio is the same.

Using these variables means once again that the design space is redundant, as any set of two values having the same ratio will correspond to the same orientation. Using these variables also helps reducing the observed dependency on initial orientations, as in Schmidt et al. (2020).

3.4 Fast post-processing

We use three termination criteria for the macro-scale topology optimization: a minimum design change as in *top88* (Andreassen et al. 2011), a maximum number of iterations since the best minimum was reached and a maximum number of overall iterations. For all the results shown in Sect. 4, the values used for these three termination criteria are respectively 0.001, 5 and 100. The iteration giving the minimum compliance is kept instead of the last one.

Once the topology optimization at the macro-scale level has converged, four variables are obtained for each cell. They are illustrated in Fig.12b in the case of an L-shaped beam. A quick post-processing step is therefore necessary to get the final design. For each macro-element, the final variables are used to find the closest cell in terms of Euclidean distance in the micro-structure database. This is immediate as the database is based on a regular grid. The micro-structure database was created off-line at the same time as the elastic tensor database. It contains the densities of the micro-elements of each micro-structure. Each macro-element in the macro-design is therefore replaced with the corresponding micro-elements. Thus a final design is obtained with full detail as in Fig. 12c.

In order to improve the connection between micro-structures and to get rid of useless elements, a second post-processing step can be added at the end of the macro-scale optimization. This post-processing is made of three steps. In the first step a full finite element analysis (FEA) is conducted on the design. This enables to access the stress in all the micro-elements. These stresses are compared to the mean stress value throughout the structure. If they are lower than a given constant (C_{post}) times this mean stress value, the elements are deleted (density set to 0) as they are considered

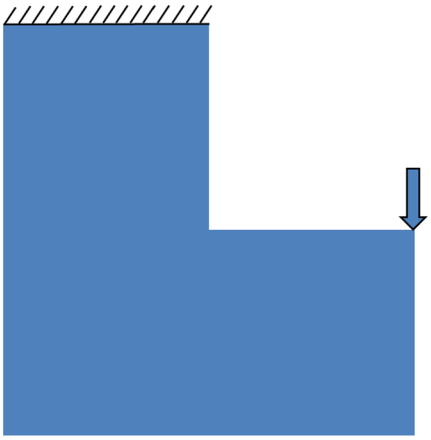

(a) The L-shaped beam problem.

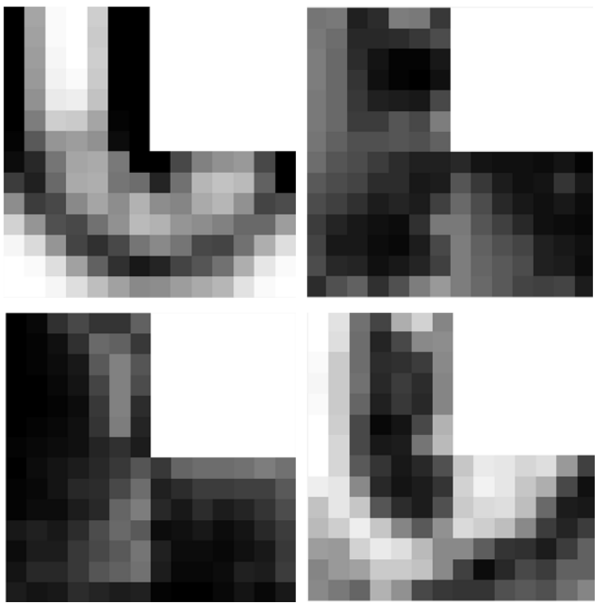

(b) The design variables at the end of the macro-optimization. The density variable is shown at the top-left, the x_{cos} variable is shown at the top-right, the x_{sin} variable is shown at the bottom-left and the cubicity variable is shown at the top-right.

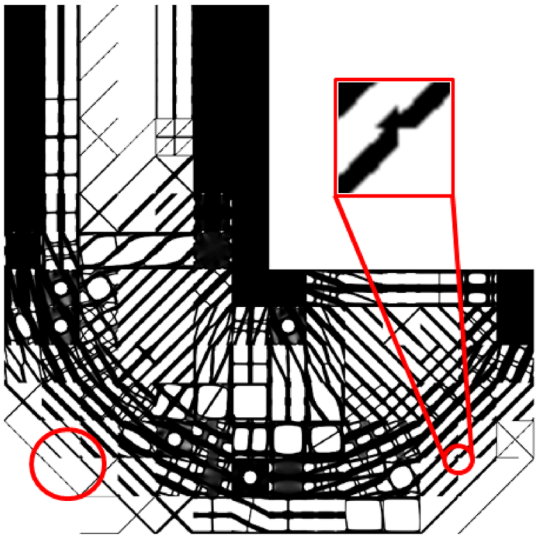

(c) The design obtained once the macro-elements are replaced by the corresponding micro-structure from the database. The circle on the left shows a zone featuring many unused elements. The circle on the right shows a zone where the connection between micro-structures is not perfect.

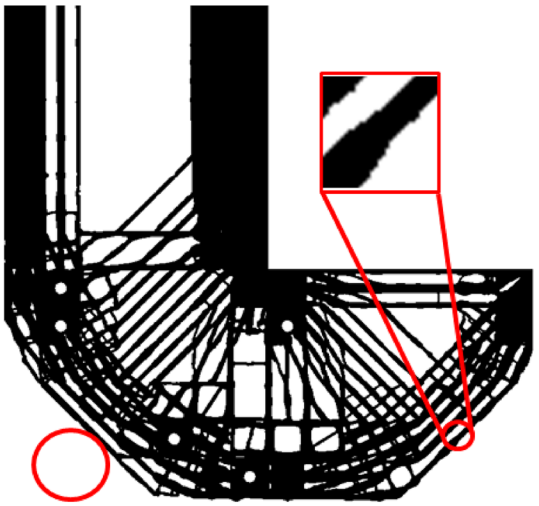

(d) The design obtained after post-processing. It can be seen that most of the useless elements have been removed and that connection between micro-structures is improved.

Fig. 12 Example showing the different steps leading from the end of the macro-optimization to the final design, in a L-shaped beam case using cells with three transmission zones per edge

to be useless. The total volume fraction of the structure therefore decreases, without having a significant impact on compliance. This step is applied three times (with C_{post1}, C_{post2} and C_{post3}). In the second step, a classical density filter (Andreassen et al. 2011; Bruns and Tortorelli 2001; Bourdin 2001) is used with a filter radius r_{post}, defined with respect to the micro-element size. This gives a minimum length scale, improving manufacturability. This step also transforms thin members into thicker grey-scale members. This is important to be able to recover the initial volume fraction in the last step. Finally all element densities are set to 0 or 1. To do this, a threshold is applied as in the code in Appendix 1: a density of 1 is assigned to all elements with a density higher than the threshold, while a density of 0 is assigned to all elements lower than this threshold. The threshold is adjusted through an iterative process to ensure that the desired volume fraction value is restored. This final step gives a physical design, as in Fig. 12d. A C_{post1} value of 1.1, C_{post2} value of 2, C_{post3}

value of 20, and r_{post} value of 4 seem to give good results in many different cases. Those values are used for all the results presented in Sect. 4. The second step, and the creation of the filter matrix for the fine-scale design in particular, is the most computationally demanding one. This step typically takes in itself twice as long as the total macro-scale topology optimization without post-processing. This illustrates the efficiency of the multi-scale topology optimisation framework.

4 Results obtained

4.1 Comparison to other strategies on classical problems

All the codes used to obtain the following results are accessible online (see Sect. 5). In all the examples presented in this paper, a global volume fraction of 0.5 was used.

EMTO is applied to classical test cases (L-shaped beam as in Fig. 12a and MBB beam) in order to compare it to other strategies. Fig. 13 shows an example of convergence graph obtained for the L-shaped beam problem on a 14×14 macro-scale grid.

We compare EMTO to *top88* in particular. According to Kumar and Suresh (2020), no method achieves clearly better results than *top88* in terms of compliance minimization. The only exception is totally free MTO as in the work of Rodrigues et al. (2002) which is very time-consuming. EMTO being much faster it is interesting to see if this limit holds.

In order to evaluate a multi-scale design properly , it is necessary to evaluate the total design, where the cells are replaced by their micro-structures (Wu et al. 2021), needing much computation time. Therefore, in order for our evaluations to be easily reproduced, we chose to compare the two methods on coarse grids of 14×14 and 30×10 macro-elements or cells for a L-shaped beam and MBB beam, respectively. Of course, this grid is too coarse for a good design to be obtained with top88, but it enables the two methods to be compared for a same number of macro-elements, and therefore compare the performance of the cells to solid/void elements, when they are included in a structure. We also compare the two methods on finer 28×28 and 60×20 grids for a fairer comparison.

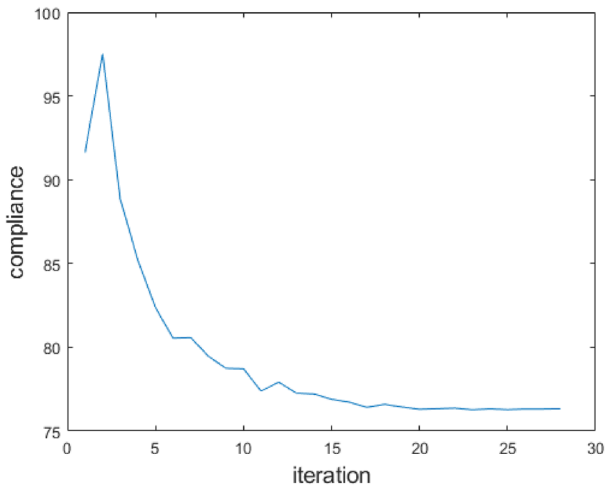

Fig. 13 Convergence graph for the L-shaped beam optimization

For each test case, a design from a mono-scale topology optimization was used as initial design. To obtain this initial design a penalization factor of 2 was used. This is a factor that gives a satisfactory approximation of our cells, based on Fig. 5. It can be seen in Figs. 14 and 15 that EMTO gives a very different design compared to classical mono-scale topology optimization, as in *top88*. However, the design shares some similarities at the macro-scale with oriented-grid methods, such as developed in Kumar and Suresh (2020), and some similarities at the micro-scale with other multi-scale methods, such as Sivapuram et al. (2016).

In order to compare the design given by EMTO to the ones given by *top88*, their compliance were evaluated with the same penalization factor ($p = 3$) and after projecting their designs on the same grid, for fairness of the comparison. The grid corresponding to the final design of EMTO (1400×1400 and 2800×2800 for the L-shaped beam, 3000×1000 and 6000×2000 for the MBB beam) was chosen as it is the more refined. The elements of the designs given by *top88* were therefore divided into smaller elements of same density in order to reach the same refinement. A filter radius of 1.5 is chosen for both *top88* and EMTO, in order for *top88* to give good results even with few elements. A sensitivity filtering is chosen for *top88*, as it also gives better results. Finally, a threshold was applied to the top88 designs to push all densities to 0 or 1, in order to avoid penalizing top88 with intermediate densities. The threshold conserving the volume fraction was chosen. For example, the command used to obtain the design in Fig. 15c is top88(30,10,0.5,3,1.5,1) followed by the application of the threshold as in the code available in Appendix 1.

The results appear in Table 1. In this table, the compliances and computation times obtained for each test case and each grid are given at three steps of the process. The computation times have been obtained using a Dell Precision 3630 desktop with an Intel Core i7-8700 processor, 32 GB memory, Windows 10, and MATLAB R2017b. The 'homogenized' step corresponds to the compliance computed at the end of the macro-optimization using homogenized stiffness tensors. It corresponds to the design in Fig. 12b. The macro-elements are not replaced by the corresponding

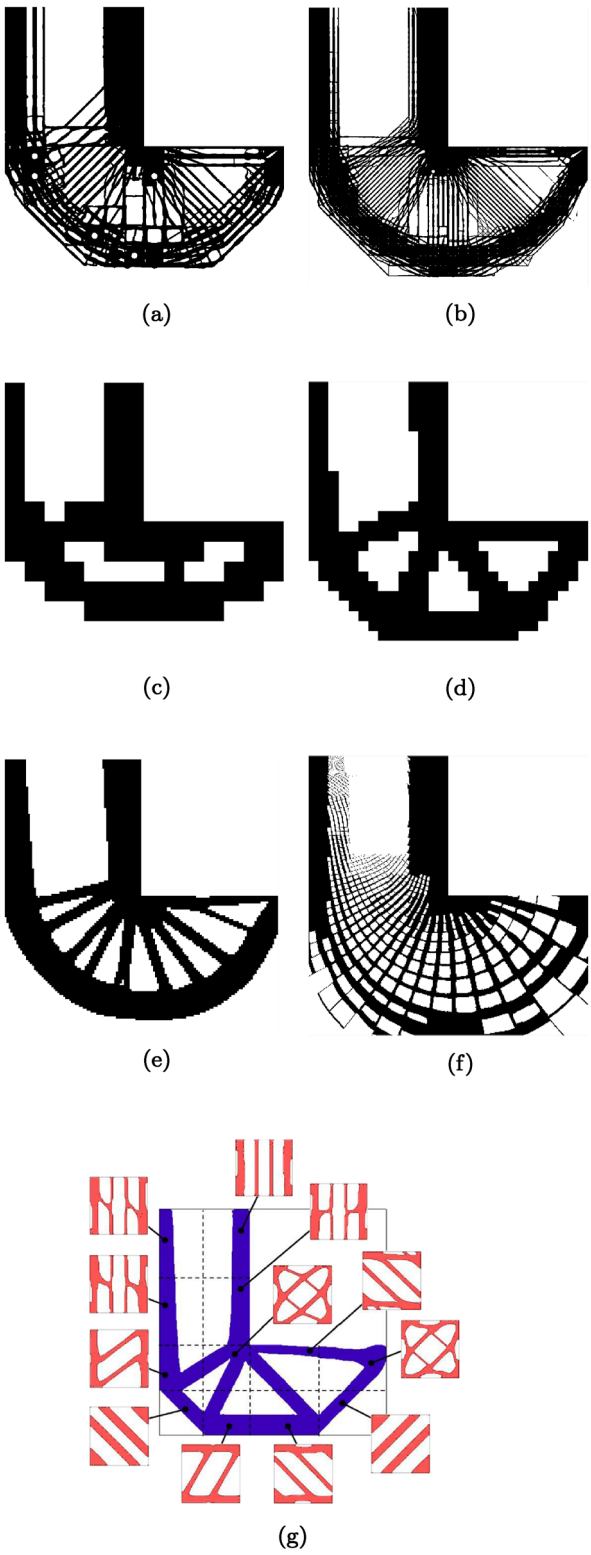

Fig. 14 Comparison of L-shaped beam designs from different methods: **a** EMTO on a 14×14 grid of cells after post-processing, **b** EMTO on a 28×28 grid of cells after post-processing, **c**, **d** *top88* with densities thresholded to 0 or 1 and with a number of elements equal to the number of macro-elements in a and b respectively, **e** *top88* with densities thresholded to 0 or 1 and with a discretization (140×140) leading to approximately the same computation time as **a**, **f** an oriented-grid method (using the code from Kumar and Suresh (2020)), **g** an alternative multi-scale method on a similar case (Sivapuram et al. 2016) ▶

micro-structures yet, so connection issues have not arisen yet. For the other two steps, the given compliances are this time the real compliances computed for the whole design, before post-processing for one (in Fig. 12c and appearing as 'no PP' in Table 1) and after post-processing for the other one (in Figs. 14a, b, 15a, b and appearing as 'with PP' in Table 1). These designs are compared to

- a *top88* problem featuring the same number of elements (147 as in Fig. 14c, 588 as in Fig. 14d, 300 as in Fig. 15c or 1200 as in Fig. 15d)
- a *top88* problem taking approximately the same time to compute

For this last *top88* problem, the number of elements is increased until the computation time is approximately as much as that needed for EMTO to reach the considered step. The example in Fig. 14e corresponds to the computation time needed to finish post-processing of the 14×14 multi-scale L-shaped beam case, whereas Fig. 15e corresponds to the computation time needed to finish post-processing of the 30×10 multi-scale MBB beam case.

EMTO is also compared to oriented-grid methods. The code published in Kumar and Suresh (2020) is used for this comparison. We find that for a same number of macro-elements (n=147), EMTO gives a compliance that is 12.8% lower on the L-shaped beam problem and is faster. On the MBB beam problem, the oriented-grid method tested doesn't give a connected design for the number of macro-elements (n=300) used with EMTO. Therefore a number of macro-elements 6.25 times higher (n=1875) is chosen for this method. The resulting design appears in Fig. 15f. Despite its lower number of macro-elements, EMTO gives a compliance that is 35.7% lower on this problem and is much faster.

It can be seen in Table 1 that the full use of EMTO (including post-processing) leads to very good results. The compliance can indeed be lowered by up to 20% on a coarse

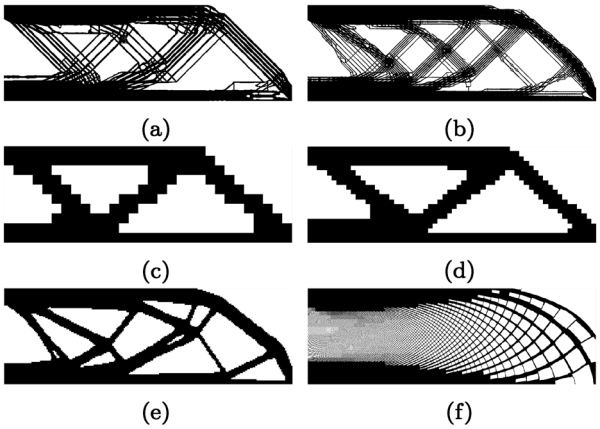

Fig. 15 Comparison of MBB beam designs from different methods: **a** EMTO on a 30×10 grid of cells after post-processing, **b** EMTO on a 60×20 grid of cells after post-processing, **c**, **d** *top88* with densities thresholded to 0 or 1 and a number of elements equal to the number of macro-elements in a and b respectively, **e** *top88* with densities thresholded to 0 or 1 and with a resolution leading to approximately the same computation time as **a**, **f** an oriented-grid method (using the code from Kumar and Suresh (2020))

14×14 grid compared to an enhanced mono-scale method where densities are forced to be 0 or 1. On a more realistic finer grid (28×28 or 60×20), the compliance can still be lowered by 3 to 4%. This is significant because for most methods, porous material is not optimal for minimum compliance design (Sivapuram et al. 2016), whereas in EMTO, porous design is always better, when the post-processing step is applied. This means that transmission zones and optimally-oriented cells are truly important. However, EMTO takes longer to run than a simple mono-scale topology optimization method. When we compare our results to those obtained with a finer mono-scale method running in the same amount of time, our advantage vanishes. It is worth noting that no particular care was taken yet in EMTO to improve our code efficiency, as this will be addressed in future work. Yet, thanks to the use of a surrogate, our computation times are not prohibitive compared to a *top88* optimization. It is interesting to consider how each step in the process affects the result :

– Replacing the theoretical cells with real micro-structures from the database increases the compliance by 20 to 40% when a coarse grid is used. Indeed, as cells are different from their neighbours, homogenization theory does not apply and the effective properties of the cells are worse than the theoretical ones.
– Applying the post-processing step enables to overcome this issue through enhanced connectivity and "smoothing" the design. As a result the compliances revert to values closer to the homogenized ones, with an increase of only 4 to 24%.
– In the cases with a finer mesh, the compliance increases only by 14 to 30% when the theoretical cells are replaced with their micro-structure. This is explained as in a finer mesh, the cells vary more smoothly and we are closer to a case where homogenization theory can apply. However, the difference between the homogenized compliances and the compliances after post-processing is much less affected by mesh refinement. Indeed, the post-processing is already designed to address the homogenization issue.

Another interesting observation is that cells with 4 transmission zones or 8 transmission zones give very similar results. The cells with 4 transmission zones preform slightly better before post-processing because they are better connected. This difference disappears after post-processing. Cells with 4 or 8 transmission zones are a good choice.

The better results obtained with EMTO using porous micro-structures than with mono-scale topology optimization, for a same number of macro-elements, can be interpreted in two ways. The first one is simply to say that designing the cells as micro-structures is equivalent to having a mono-scale design with more elements. This interpretation is illustrated in Fig. 16 where the compliance obtained using EMTO is compared to mono-scale designs with different number of elements, on the MBB beam case. All the designs are evaluated on a 3000×1000 grid, as in Table 1. The element densities of the *top88* cases are thresholded to 0 or 1 as previously described. Graphically, it can be seen that with post-processing, EMTO gives results close to a mono-scale method using 11 times more elements. This is easy to understand, as our micro-structures are made of 100×100 micro-elements. In fact, results closer to a mono-scale method featuring 10 000 times more elements could have been expected, but some of the improvement given by this high resolution is lost in micro-structure connection and reduced design space.

Another interpretation of the result improvement is that using porous micro-structures is equivalent to having a lower penalization. This interpretation is illustrated in Fig. 17 where the compliance obtained using *top88* is plotted for different penalization factors from 1 to 3. In this figure, no 0/1 thresholding is applied, except on the blue dot, in order to see the effect of penalization. The compliance obtained

Table 1 Comparison of compliances from our results vs *top88* for different problems, grids, number of transmission zones (TZ), different steps in the method and for different equivalent *top88* cases

Problem	Step	Macro-grid	Evaluation grid	Time (s)	c	vs *top88* Same Macro-grid	vs *top88* Same time (Compliance, grid)
L-shaped top88	–	14×14 (Fig. 14c)	1400×1400	1	119.2	–	–
L-shaped 8TZ	Homogenized	14×14	–	10	76.3	− 36.0	− 13.2% (87.9, 70×70)
L-shaped 4TZ	Homogenized	14×14	–	9	76.3	− 36.0	− 13.2% (87.9, 70×70)
L-shaped 8TZ	No PP	14×14	1400×1400	15	108.6	− 8.9	+ 24.4% (87.3, 88×88)
L-shaped 4TZ	No PP	14×14	1400×1400	15	104.9	− 12.0	+ 20.2% (87.3, 88×88)
L-shaped 8TZ	With PP	14×14	1400×1400	56	94.3	− 20.9	+ 9.3% (86.3, 140×140, Fig. 14e)
L-shaped 4TZ	With PP	14×14	1400×1400	52	94.5	− 20.7	+ 9.5% (86.3, 140×140, Fig. 14e)
L-shaped top88	–	28×28 (Fig. 14d)	2800×2800	1	93.6	–	–
L-shaped 8TZ	Homogenized	28×28	–	38	75.9	− 18.9	− 13.8% (88.1, 122×122)
L-shaped 4TZ	Homogenized	28×28	–	40	75.8	− 19.0	− 14.0% (88.1, 122×122)
L-shaped 8TZ	No PP	28×28	2800×2800	45	97.9	+ 4.6	+ 11.3% (88.0, 134×134)
L-shaped 4TZ	No PP	28×28	2800×2800	47	96.6	+ 3.2	+ 9.8% (88.0, 134×134)
L-shaped 8TZ	With PP	28×28	2800×2800	230	90.7	− 3.1	+ 3.4% (87.7, 280×280)
L-shaped 4TZ	With PP	28×28	2800×2800	234	90.6	− 3.2	+ 3.3% (87.7, 280×280)
MBB top88	–	30×10 (Fig. 15c)	3000×1000	1	223.4	–	–
MBB 8TZ	Homogenized	30×10	–	15	196.6	− 12.0	− 1.7% (199.9, 120×40)
MBB 4TZ	Homogenized	30×10	–	20	196.4	− 12.1	− 1.1% (198.4, 150×50)
MBB 8TZ	No PP	30×10	3000×1000	20s	234.8	+ 5.1	+ 18.3% (198.4, 150×50)
MBB 4TZ	No PP	30×10	3000×1000	25	216.3	− 3.2	+ 9.0% (198.4, 150×50)
MBB 8TZ	With PP	30×10	3000×1000	78	203.8	− 8.8	+ 3.9% (196.1, 231×77, Fig. 15e)
MBB 4TZ	With PP	30×10	3000×1000	81	201.9	− 9.6	+ 3.0% (196.1, 231×77, Fig. 15e)
MBB top88	–	60×20 (Fig. 15d)	6000×2000	2	211.7	–	–
MBB 8TZ	Homogenized	60×20	–	47	195.0	− 7.9	− 1.9% (198.8, 201×67)
MBB 4TZ	Homogenized	60×20	–	49	195.1	− 7.8	− 1.9% (198.8, 201×67)
MBB 8TZ	No PP	60×20	6000×2000	52s	221.5	+ 4.6	+ 11.4% (198.8, 201×67)
MBB 4TZ	No PP	60×20	6000×2000	55	212.2	+ 0.2	+ 6.7% (198.8, 201×67)
MBB 8TZ	With PP	60×20	6000×2000	340	202.3	− 4.4	+ 1.5% (199.4, 429×143)
MBB 4TZ	With PP	60×20	6000×2000	272	201.6	− 4.8	+ 1.3% (199.1, 375×125)

The *top88* designs are thresholded to full/void elements to enhance their performance. A negative percentage means that performance is improved. The step after post-processing is the most relevant for EMTO. It can be observed that compliance can be diminished through EMTO (up to 20% on a toy case or 4% on a more realistic case) compared to a mono-scale topology optimization with the same number of elements

with EMTO with a penalization factor of 3 on the micro-elements is also plotted for comparison. Generally, comparison between isotropic and anisotropic material stiffness to weight ratio strongly depends on loading. Therefore, this comparison is done on three different loading cases: an MBB beam with a 60×20 grid, an L-shaped beam with a 28×28 grid, and a cantilever beam with a 40×20 grid. All the designs are evaluated on a higher resolution grid featuring 10 000 times more elements in order to evaluate the full multi-scale design. It can be seen that, in these mono-loading cases, using EMTO with post-processing gives results similar to a mono-scale topology optimization with a penalization factor between 1.3 and 1.5. This can be understood by looking back at Fig. 5. Indeed, orienting the material inside the cells enables to have performances corresponding to a lower penalization factor. However, the data points for *top88* with 0/1 thresholding shows that some of the improvement is simply obtained through post-processing. Moreover this equivalent penalization factor may not be observed for more complex cases such as with multiple loads.

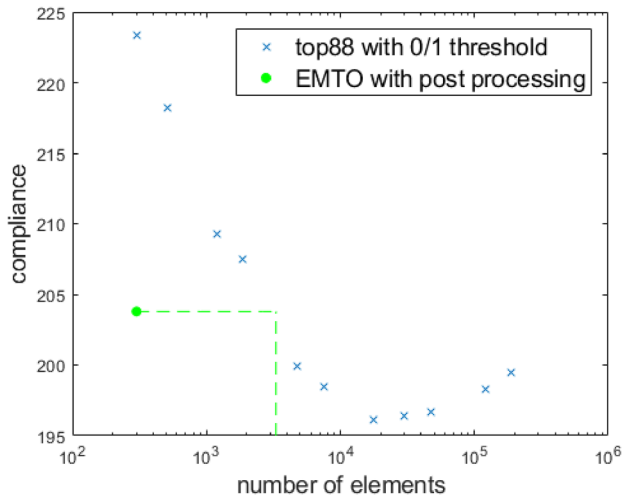

Fig. 16 Comparison of the compliances obtained with EMTO and with *top88* for different numbers of elements. All the optimizations are conducted with a penalization factor of 3 and evaluated on a 3000×1000 high-resolution grid, as in the coarse case of Table 1. For EMTO, the macro-grid has 300 elements. Graphically, the results of EMTO with post-processing are equivalent to an increase in the number of elements by a factor of 11

4.2 A versatile framework for other constraints

In the previous examples, small-size macro-grids of the order of 150 to 1200 elements were used. It is of course possible to use finer grids for finer designs. This gives better results and in general reduces the need for post-processing. Indeed, if the filter radius is also increased, variables vary more smoothly from a cell to its neighbour and conditions are therefore closer to those enabling homogenization theory. An example of a high definition design can be seen in Fig. 18 for a cantilever beam problem. However, this gives a design represented by a matrix too large to compute the compliance of the full structure at micro-scale level with the limited memory computing resources used. Therefore, only theoretical compliance from the macro-scale optimization is accessible in this case.

The method presented in this paper (EMTO) is very versatile and can accommodate various problems or constraints. This versatility is due in particular to the design variables presented in Sect. 2.1. Three examples of new problems are presented in the rest of this section: controlled porosity, fixed topology, and fixed orientation. All these problems are easily run by changing only the bounds of the design variables.

A first problem that can be treated with EMTO is a case where porosity is constrained. For example, it is possible to easily impose a same porosity (p_{fixed}) to all the micro-structures as in Eq. (10a) or a minimum porosity (p_{min}) by imposing limits on the density variable (x_{dens}) as in Eq. (10b).

$$x_{\text{dens}} = 1 - p_{\text{fixed}} \tag{10a}$$

$$x_{\text{dens}} \leq 1 - p_{\text{min}} \tag{10b}$$

Example of designs obtained with such constraints appears in Fig. 19.

EMTO can also accommodate a case where the topology is fixed. In this case, only the orientation and cubicity variables are fixed and only the density varies. This is illustrated in Fig. 20a for an orientation angle of $\pi/4$ and a cubicity of 0.5. This gives designs that are similar to other works in literature (Fig.20b from Li et al. (2017)).

Another possibility is to fix only the orientation variable, which can help achieve designs more easily manufactured at small scales, where the features of the design would be aligned with the printing path. This is illustrated in Fig. 20c, for an orientation angle of $\pi/4$.

5 Conclusion

In this paper, a new efficient multi-scale topology optimization (EMTO) method is proposed in order to address recurrent issues such as high computational costs, connectivity issues and lower performance due to reduced design spaces. EMTO uses micro-structures that are well connected through adaptable transmission zones, which limit loss of performance. Although a regular, non-oriented-grid is proposed, the micro-structure is oriented inside each cell to enable better performance. In order to speed up the process, a surrogate model is used both for the cell elastic tensor and for the cell micro-structure. For design on small grids, where cells vary rapidly, a post-processing is used to improve connectivity. It is shown that EMTO achieves significant improvements (up to 20% on a simplistic case or 4% on a more realistic case) compared to mono-scale methods on the same grid, and is promising in terms of speed. Future work includes speeding up the macro-optimization and post-processing, generalizing

Fig. 17 Comparison of the compliances obtained with EMTO and with *top88* for different penalization factors. The *top88* designs where densities are thresholded to 0 or 1 and with a penalization of 3, corresponding to Figs. 14d and 15d are added for reference. All the other *top88* points correspond to designs were the final intermediate densities (grey elements) are left unchanged. For EMTO, the micro-elements penalization factor is $p = 3$. Graphically, the results of EMTO are equivalent to using a penalization factor between 1.3 and 1.5 instead of 3, in the different loading cases studied

to a 3-d case and to other problem formulations featuring stress or manufacturing constraints.

Appendix 1: Code for thresholding densities to 0 or 1

```
function xPhys01=threshold01(xPhys,volfrac)
  xPhys01=xPhys;
  lowlim=0;
  highlim=1;
  difVF=1;
while difVF>0.0001 && highlim - lowlim > 0.000001
  midlim=(lowlim + highlim)/2;
  xPhys01(xPhys>=midlim)=1;
  xPhys01(xPhys<midlim)=0;
  volfrac01=mean(mean(xPhys01));
  difVF=abs(volfrac01 - volfrac);
  if volfrac01<volfrac
    highlim=midlim;
  else
    lowlim=midlim;
  end
 end
end
```

Appendix 2: Initial designs used in micro-structure optimization multi-start strategy

The different initial designs in Figs. 21 and 22 were used as part of the micro-structure optimization multi-start strategy. Each of these designs was the best initial design for at least one of the points in the database.

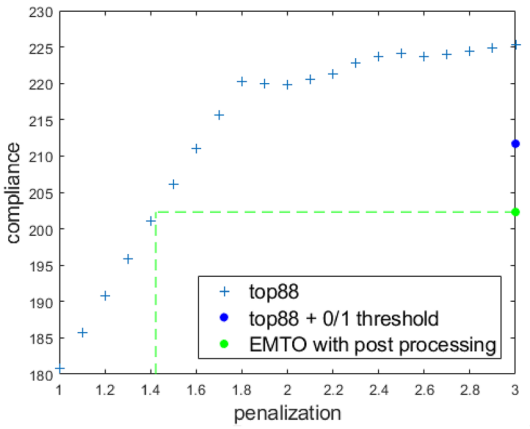

(a) MBB beam loading case. All the optimisations are conducted on a 60*20 grid of elements (*top88*) or cells (multi-scale method). The design is evaluated on a 6000*2000 grid in each case.

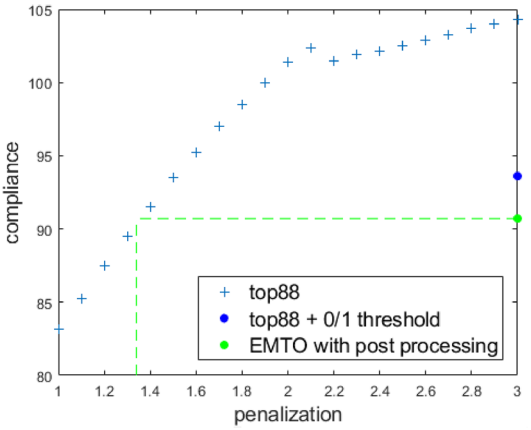

(b) L-shaped beam loading case. All the optimisations are conducted on a 28*28 grid of elements (*top88*) or cells (multi-scale method) and the final design is evaluated on a 2800*2800 grid in each case.

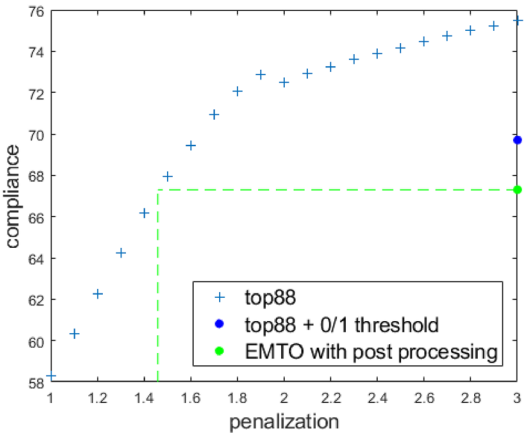

(c) Cantilever beam loading case. All the optimisations are conducted on a 40*20 grid of elements (*top88*) or cells (multi-scale method) and the final design is evaluated on a 4000*2000 grid in each case.

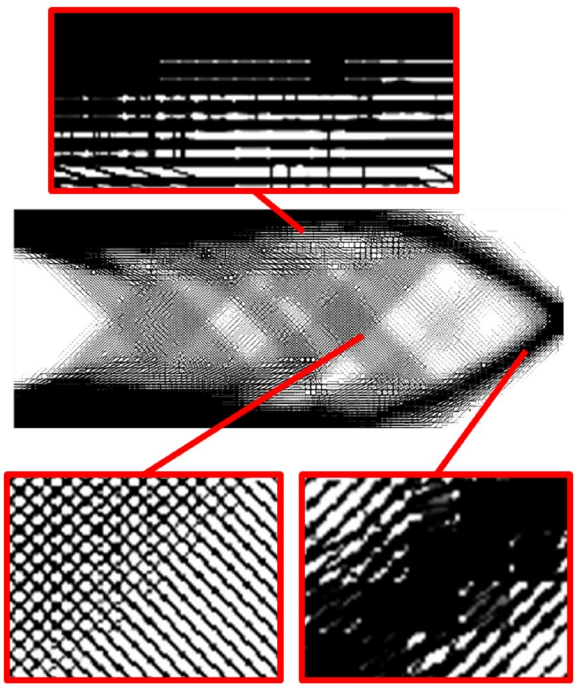

Fig. 18 High-resolution design obtained for a cantilever beam on a 100 by 40 elements grid. Cells with 3 transmission zones per edge are used, and no post-processing is applied. Theoretical compliance is 115

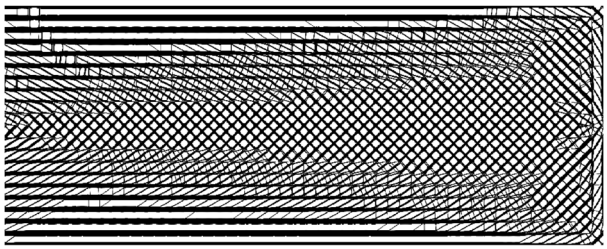

(a) Design obtained for a cantilever beam when porosity is fixed to 0.5 for every micro-structure. Cells with 2 transmission zones per edge are used, and no post-processing is applied. The theoretical compliance is 170.

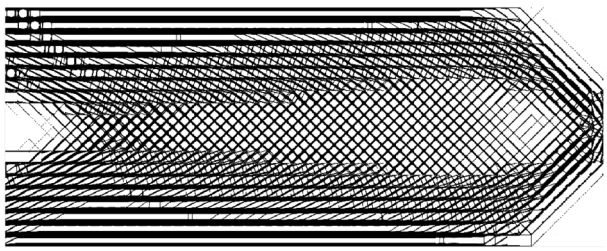

(b) Design obtained for a cantilever beam where a minimum porosity of 0.4 is applied. Cells with 2 transmission zones per edge are used, and no post-processing is applied. The theoretical compliance is 148.

Fig. 19 Example of designs for a cantilever beam obtained with constraints on porosity

Appendix 3: Input–output examples from the database

Three random sets of input were tested on the database to exemplify how it works. The database of cells with 3 transmission zones per edge is used. The inputs appear on the left in Figs. 23, 24 and 25. The top input is density, the second input is orientation (in radians), and the lowest input is cubicity, as in Fig. 8. The output tensors and micro-structures appear on the right in those figures.

Fig. 20 Example of designs for a cantilever beam obtained by limiting the design space

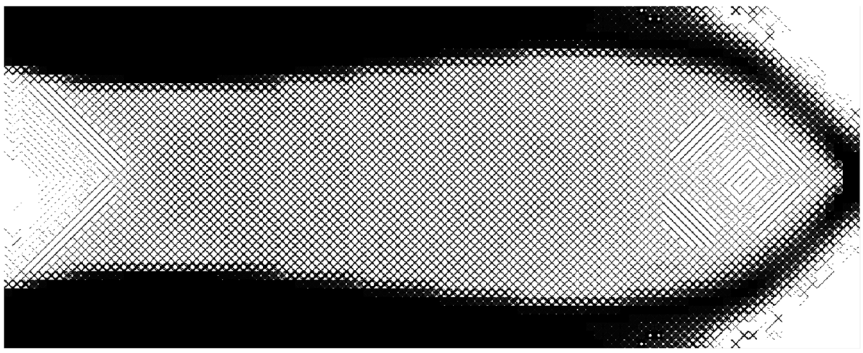

(a) Design obtained when varying only the density. Cells with 2 transmission zones per edge are used, and no post-processing is applied. The theoretical compliance is 123.

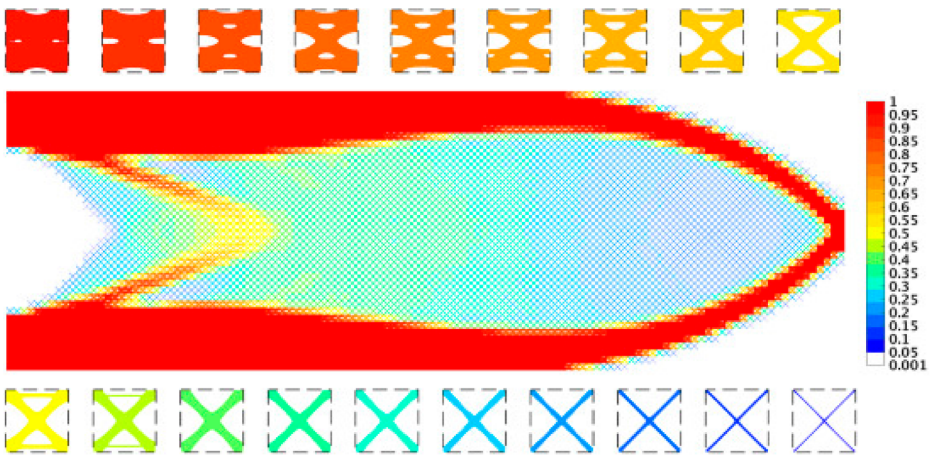

(b) Design obtained through a method based on density-clustering (Li et al. (2017))

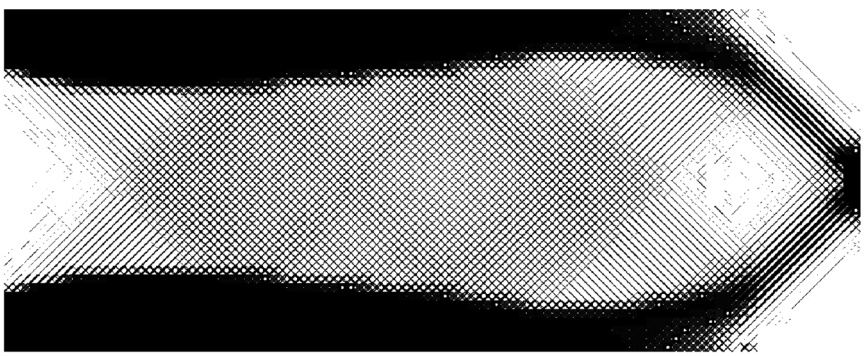

(c) Design obtained when only orientation is fixed. Cells with 2 transmission zones per edge are used, and no post-processing is applied. The theoretical compliance is 121.

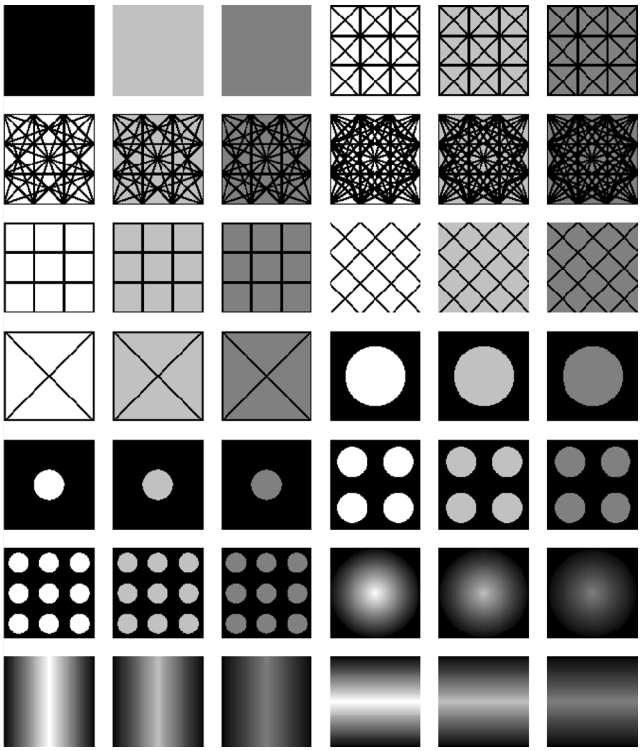

Fig. 21 Initial designs for cells with 2 transmission zones per edge

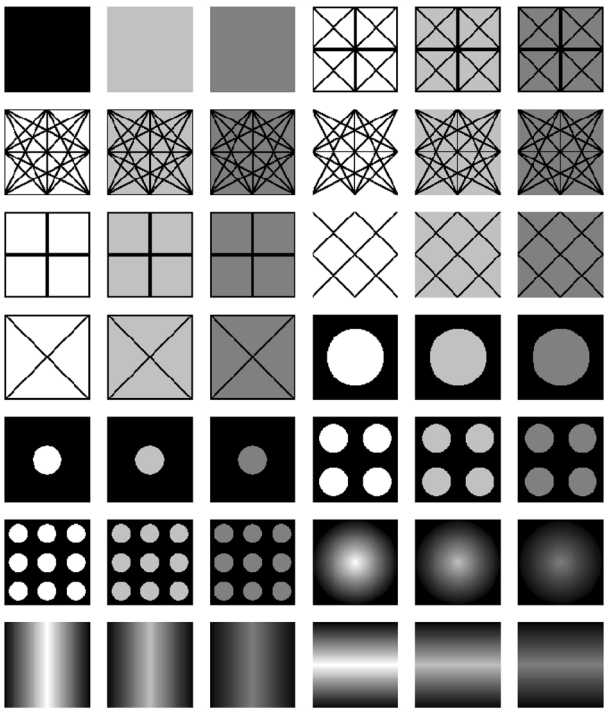

Fig. 22 Initial designs for cells with 3 transmission zones per edge

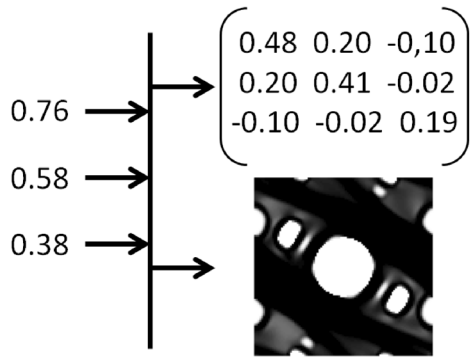

Fig. 23 Random database example 1

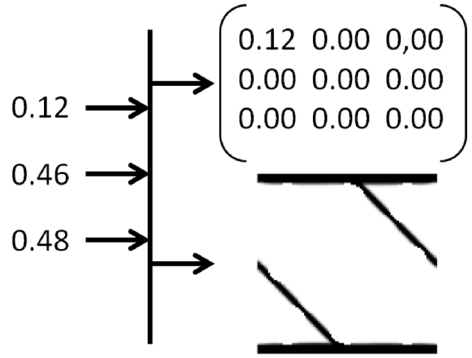

Fig. 24 Random database example 2

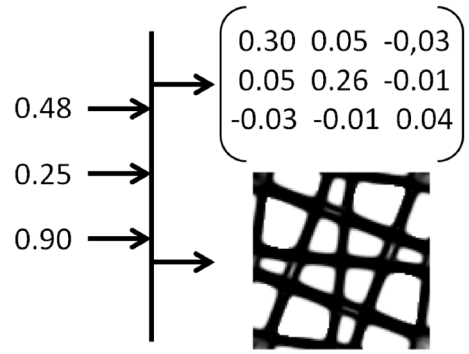

Fig. 25 Random database example 3

Acknowledgements The authors would like to thank École polytechnique for funding this research through an AMX PhD fund.

The authors also thank Krister Svanberg for providing the MATLAB MMA code, and Julien Pedron for his help with the computer Pando.

Declarations

Conflict of interest The authors declare that they have no conflict of interest.

Replication of results All the codes and material used to obtain the results presented in this paper can be found at https://github.com/mid2SUPAERO/EMTO. This includes the databases and the code to build them.

References

Allaire G, Geoffroy-Donders P, Pantz O (2019) Topology optimization of modulated and oriented periodic microstructures by the homogenization method. Comput Math Appl 78(7):2197–2229. https://doi.org/10.1016/j.camwa.2018.08.007

Andreassen E, Clausen A, Schevenels M, Lazarov BS, Sigmund O (2011) Efficient topology optimization in MATLAB using 88 lines of code. Struct Multidisc Optim 43(1):1–16. https://doi.org/10.1007/s00158-010-0594-7

Avellaneda M (1987) Optimal bounds and microgeometries for elastic two-phase composites. SIAM J Appl Math 47(6):1216–1228. https://doi.org/10.1137/0147082

Bendse MP (1989) Optimal shape design as a material distribution problem. Struct Optim 1:193–202. https://doi.org/10.1007/BF01650949

Bendse MP, Kikuchi N (1988) Generating optimal topologies in structural design using a homogenization method. Comput Methods Appl Mech Eng 71(2):197–224. https://doi.org/10.1016/0045-7825(88)90086-2

Bendsoe MP, Sigmund O (2004) Topology optimization: theory, methods, and applications, 2nd edn. Springer, Berlin, Heidelberg. https://doi.org/10.1007/978-3-662-05086-6

Bendsoe MP, Guedes JM, Haber RB, Pedersen P, Taylor JE (1994) An analytical model to predict optimal material properties in the context of optimal structural design. J Appl Mech 61(4):930–937. https://doi.org/10.1115/1.2901581

Bouhlel MA, Hwang JT, Bartoli N, Lafage R, Morlier J, Martins JRRA (2019) A Python surrogate modeling framework with derivatives. Adv Eng Softw. https://doi.org/10.1016/j.advengsoft.2019.03.005

Bourdin B (2001) Filters in topology optimization. Int J Numer Methods Eng 50(9):2143–2158. https://doi.org/10.1002/nme.116. https://onlinelibrary.wiley.com/doi/abs/10.1002/nme.116

Bruns TE, Tortorelli DA (2001) Topology optimization of non-linear elastic structures and compliant mechanisms. Comput Methods Appl Mech Eng 190(26):3443–3459. https://doi.org/10.1016/S0045-7825(00)00278-4. https://www.sciencedirect.com/science/article/pii/S0045782500002784

Coelho PG, Fernandes PR, Guedes JM, Rodrigues HC (2008) A hierarchical model for concurrent material and topology optimisation of three-dimensional structures. Struct Multidisc Optim 35(2):107–115. https://doi.org/10.1007/s00158-007-0141-3

Coniglio S, Morlier J, Gogu C, Amargier R (2019) Generalized geometry projection: a unified approach for geometric feature based topology optimization. Arch Comput Methods Eng. https://doi.org/10.1007/s11831-019-09362-8

Deng J, Yan J, Cheng G (2013) Multi-objective concurrent topology optimization of thermoelastic structures composed of homogeneous porous material. Struct Multidisc Optim. https://doi.org/10.1007/s00158-012-0849-6

Du Z, Zhou XY, Picelli R, Kim HA (2018) Connecting microstructures for multiscale topology optimization with connectivity index constraints. J Mech Des 10(1115/1):4041176

Ferrer A, Cante JC, Hernández JA, Oliver J (2018) Two-scale topology optimization in computational material design: an integrated approach. Int J Numer Methods Eng 114(3):232–254. https://doi.org/10.1002/nme.5742

Garner E, Kolken H, Wang C, Zadpoor A, Wu J (2018) Compatibility in microstructural optimization for additive manufacturing. Addit Manuf 26:65–75. https://doi.org/10.1016/j.addma.2018.12.007

Groen JP, Sigmund O (2018) Homogenization-based topology optimization for high-resolution manufacturable microstructures: Homogenization-based topology optimization for high-resolution manufacturable microstructures. Int J Numer Methods Eng 113(8):1148–1163. https://doi.org/10.1002/nme.5575

Guo X, Zhang W, Zhong W (2014) Doing topology optimization explicitly and geometrically—a new moving morphable components based framework. J Appl Mech 10(1115/1):4027609

Hashin Z, Shtrikman S (1962) A variational approach to the theory of the elastic behaviour of polycrystals. J Mech Phys Solids 10(4):343–352. https://doi.org/10.1016/0022-5096(62)90005-4

Huang X, Radman A, Xie YM (2011) Topological design of microstructures of cellular materials for maximum bulk or shear modulus. Comput Mater Sci 50(6):1861–1870. https://doi.org/10.1016/j.commatsci.2011.01.030

Hu J, Li M, Yang X, Gao S (2020) Cellular structure design based on free material optimization under connectivity control. Comput Aided Des. https://doi.org/10.1016/j.cad.2020.102854. https://linkinghub.elsevier.com/retrieve/pii/S0010448520300476

Imediegwu C, Murphy R, Hewson R, Santer M (2019) Multiscale structural optimization towards three-dimensional printable structures. Struct Multidisc Optim 60(2):513–525. https://doi.org/10.1007/s00158-019-02220-y

Jia J, Da D, Loh CL, Zhao H, Yin S, Xu J (2020) Multiscale topology optimization for non-uniform microstructures with hybrid cellular automata. Struct Multidisc Optim 62(2):757–770. https://doi.org/10.1007/s00158-020-02533-3

Jog CS, Haber RB, Bendsøe MP (1994) Topology design with optimized, self-adaptive materials. Int J Numer Methods Eng 37(8):1323–1350. https://doi.org/10.1002/nme.1620370805

Kumar T, Suresh K (2020) A density-and-strain-based K-clustering approach to microstructural topology optimization. Struct Multidisc Optim 61(4):1399–1415. https://doi.org/10.1007/s00158-019-02422-4

Kumar T, Sridhara S, Prabhune B, Suresh K (2021) Spectral decomposition for graded multi-scale topology optimization. Comput Methods Appl Mech Eng. https://doi.org/10.1016/j.cma.2021.113670. https://www.sciencedirect.com/science/article/pii/S0045782521000062

Li H, Luo Z, Gao L, Qin Q (2017) Topology optimization for concurrent design of structures with multi-patch microstructures by level sets. Comput Methods Appl Mech Eng. https://doi.org/10.1016/j.cma.2017.11.033

Li D, Liao W, Dai N, Xie YM (2020) Anisotropic design and optimization of conformal gradient lattice structures. Comput Aided Des. https://doi.org/10.1016/j.cad.2019.102787

Liu L, Yan J, Cheng G (2008) Optimum structure with homogeneous optimum truss-like material. Comput Struct 86(13):1417–1425. https://doi.org/10.1016/j.compstruc.2007.04.030

Liu P, Kang Z, Luo Y (2020a) Two-scale concurrent topology optimization of lattice structures with connectable microstructures. Addit Manuf. https://doi.org/10.1016/j.addma.2020.101427

Liu Z, Xia L, Xia Q, Shi T (2020b) Data-driven design approach to hierarchical hybrid structures with multiple lattice configurations. Struct Multidisc Optim. https://doi.org/10.1007/s00158-020-02497-4

Li Q, Xu R, Wu Q, Liu S (2021) Topology optimization design of quasi-periodic cellular structures based on erode-dilate operators. Comput Methods in Mech Eng. https://doi.org/10.1016/j.cma.2021.113720. https://www.sciencedirect.com/science/article/pii/S0045782521000566

Luo Y, Hu J, Liu S (2021) Self-connected multi-domain topology optimization of structures with multiple dissimilar microstructures. Struct Multidisc Optim. https://doi.org/10.1007/s00158-021-02865-8

Nadaraya EA (1964) On estimating regression. Theory Probab Appl 9(1):141–142. https://doi.org/10.1137/1109020

Norato JA (2018) Topology optimization with supershapes. Struct Multidisc Optim 58(2):415–434. https://doi.org/10.1007/s00158-018-2034-z

Qiu Z, Li Q, Liu S, Xu R (2020) Clustering-based concurrent topology optimization with macrostructure, components, and materials. Struct Multidisc Optim. https://doi.org/10.1007/s00158-020-02755-5

Rodrigues H, Guedes J, Bendsoe M (2002) Hierarchical optimization of material and structure. Struct Multidisc Optim 24(1):1–10. https://doi.org/10.1007/s00158-002-0209-z

Schmidt MP, Couret L, Gout C, Pedersen CBW (2020) Structural topology optimization with smoothly varying fiber orientations. Struct Multidisc Optim 62(6):3105–3126. https://doi.org/10.1007/s00158-020-02657-6

Sigmund O (1994) Materials with prescribed constitutive parameters: an inverse homogenization problem. Int J Solids Struct 31(17):2313–2329. https://doi.org/10.1016/0020-7683(94)90154-6

Sigmund O, Torquato S (1997) Design of materials with extreme thermal expansion using a three-phase topology optimization method. J Mech Phys Solids 45(6):1037–1067. https://doi.org/10.1016/S0022-5096(96)00114-7

Sivapuram R, Dunning PD, Kim HA (2016) Simultaneous material and structural optimization by multiscale topology optimization. Struct Multidisc Optim 54(5):1267–1281. https://doi.org/10.1007/s00158-016-1519-x

Stutz FC, Groen JP, Sigmund O, Bærentzen JA (2020) Singularity aware de-homogenization for high-resolution topology optimized structures. Struct Multidisc Optim 62(5):2279–2295. https://doi.org/10.1007/s00158-020-02681-6

Svanberg K (1987) The method of moving asymptotes-a new method for structural optimization. Int J Numer Methods Eng 24(2):359–373. https://doi.org/10.1002/nme.1620240207. https://onlinelibrary.wiley.com/doi/abs/10.1002/nme.1620240207

Wang MY, Wang X, Guo D (2003) A level set method for structural topology optimization. Comput Methods Appl Mech Eng 192(1):227–246. https://doi.org/10.1016/S0045-7825(02)00559-5

Wang Y, Chen F, Wang MY (2017a) Concurrent design with connectable graded microstructures. Comput Methods Appl Mech Eng 317:84–101. https://doi.org/10.1016/j.cma.2016.12.007

Wang Y, Xu H, Pasini D (2017b) Multiscale isogeometric topology optimization for lattice materials. Comput Methods Appl Mech Eng 316:568–585. https://doi.org/10.1016/j.cma.2016.08.015

Wang C, Zhu JH, Zhang WH, Li SY, Kong J (2018) Concurrent topology optimization design of structures and non-uniform parameterized lattice microstructures. Struct Multidisc Optim 58(1):35–50. https://doi.org/10.1007/s00158-018-2009-0

Wang C, Gu X, Zhu J, Zhou H, Li S, Zhang W (2020) Concurrent design of hierarchical structures with three-dimensional parameterized lattice microstructures for additive manufacturing. Struct Multidisc Optim. https://doi.org/10.1007/s00158-019-02408-2

Watts S, Arrighi W, Kudo J, Tortorelli DA, White DA (2019) Simple, accurate surrogate models of the elastic response of three-dimensional open truss micro-architectures with applications to multiscale topology design. Struct Multidisc Optim 60(5):1887–1920. https://doi.org/10.1007/s00158-019-02297-5

White DA, Arrighi WJ, Kudo J, Watts SE (2019) Multiscale topology optimization using neural network surrogate models. Comput Methods Appl Mech Eng 346:1118–1135. https://doi.org/10.1016/j.cma.2018.09.007. https://www.sciencedirect.com/science/article/pii/S004578251830450X

Wu J, Sigmund O, Groen JP (2021) Topology optimization of multi-scale structures: a review. Struct Multidisc Optim 63(3):1455–1480. https://doi.org/10.1007/s00158-021-02881-8

Xia L, Breitkopf P (2015a) Design of materials using topology optimization and energy-based homogenization approach in Matlab. Struct Multidisc Optim 52(6):1229–1241. https://doi.org/10.1007/s00158-015-1294-0

Xia L, Breitkopf P (2015b) Multiscale structural topology optimization with an approximate constitutive model for local material microstructure. Comput Methods Appl Mech Eng 286:147–167. https://doi.org/10.1016/j.cma.2014.12.018

Xia L, Xia Q, Huang X, Xie YM (2018) Bi-directional evolutionary structural optimization on advanced structures and materials: a comprehensive review. Arch Comput Methods Eng 25(2):437–478. https://doi.org/10.1007/s11831-016-9203-2

Xie YM, Steven GP (1993) A simple evolutionary procedure for structural optimization. Comput Struct 49(5):885–896. https://doi.org/10.1016/0045-7949(93)90035-C

Xie YM, Yang X, Shen J, Yan X, Ghaedizadeh A, Rong J, Huang X, Zhou S (2014) Designing orthotropic materials for negative or zero compressibility. Int J Solids Struct 51(23):4038–4051. https://doi.org/10.1016/j.ijsolstr.2014.07.024

Xu L, Cheng G (2018) Two-scale concurrent topology optimization with multiple micro materials based on principal stress orientation. Struct Multidisc Optim. https://doi.org/10.1007/s00158-018-1916-4

Yan X, Huang X, Zha Y, Xie YM (2014) Concurrent topology optimization of structures and their composite microstructures. Comput Struct 133:103–110. https://doi.org/10.1016/j.compstruc.2013.12.001

Zhou S, Li Q (2008) Design of graded two-phase microstructures for tailored elasticity gradients. J Mater Sci 43:5157–5167. https://doi.org/10.1007/s10853-008-2722-y

Zhou XY, Du Z, Kim HA (2019) A level set shape metamorphosis with mechanical constraints for geometrically graded microstructures. Struct Multidisc Optim 60(1):1–16. https://doi.org/10.1007/s00158-019-02293-9

Zhu B, Skouras M, Chen D, Matusik W (2017) Two-scale topology optimization with microstructures. arXiv:170603189